
Not All Tokens Learn Alike: Attention Entropy Reveals Heterogeneous Signals in RL Reasoning

Gengyang Li^{1,3}, Zheng-Fan Wu^{1,†}, Siqi Bao^{1,†}, Yunfang Wu^{2,†}

¹Baidu

²School of Computer Science, Peking University

³School of Software and Microelectronics, Peking University

ligengyang@stu.pku.edu.cn

{wuzhengfan, baosiqi}@baidu.com, wuyf@pku.edu.cn

Abstract

Reinforcement-learning-based post-training has become a central paradigm for improving the reasoning ability of large language models, yet the structure of its token-level learning signals remains poorly understood. This work studies such heterogeneity through attention entropy, a diagnostic that measures how concentrated or diffuse the contextual support is for each response token.

We first show that token-level RL objectives are sparsely estimable: uniformly random 20% token subsets preserve a substantial fraction of full-token held-out performance, suggesting considerable redundancy in token-level updates. However, entropy-structured subsets exhibit markedly different optimization behavior. Low-attention-entropy tokens, which we call anchors, rely on concentrated support, produce stable gradients aligned with full-token updates, and provide a reliable optimization backbone, but they tend to plateau on harder benchmarks. High-attention-entropy tokens, which we call explorers, aggregate more diffuse context and induce larger but directionally more volatile gradients. Explorer-only training is unstable on average, yet the rare trajectories that avoid collapse suggest that these tokens can contain useful hard-reasoning signals when optimization remains stable.

We substantiate this anchor–explorer spectrum through evidence-gathering analyses, entropy dynamics, gradient-geometry diagnostics, and controls showing that position, predictive entropy, and loss normalization do not explain the observed training asymmetry. Finally, a dynamic entropy-aware soft-reweighting intervention improves Qwen3-8B-Base from 34.39 to 37.40 held-out average in the strongest entropy-source setting, with representative shallow, middle, and deep layers all outperforming full-token DAPO while favoring different benchmarks. These findings suggest that attention entropy reveals optimization-relevant structure in token-level RL signals, and that uniform token averaging can obscure meaningful heterogeneity in RL-based reasoning post-training.

1 Introduction

Reinforcement-learning-based post-training has become central to improving reasoning in large language models, but its token-level learning signal remains poorly understood. A single verifiable outcome reward is distributed across a long reasoning trace, yet the induced token updates need not have the same quality: some may preserve local fluency, others may stabilize intermediate states, and others may connect distant evidence. Uniform token averaging treats these contributions as

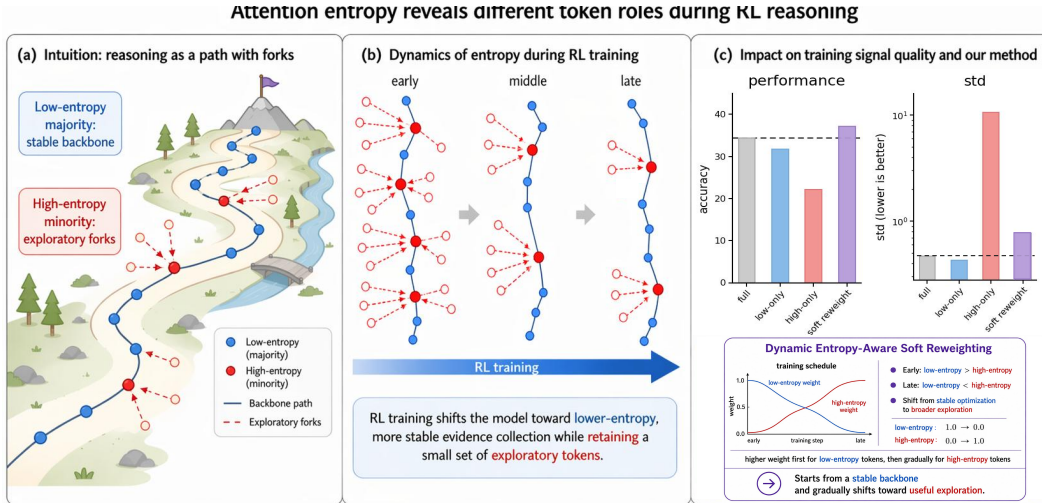


Figure 1: Attention entropy reveals an optimization spectrum in RL reasoning training. (a) Tokens span a spectrum from **anchor tokens** (low entropy, sparse selective support) to **explorer tokens** (high entropy, diffuse multi-position aggregation). (b) Selective training exposes the spectrum: anchor-only training is stable but plateaus; explorer-only training is fragile overall, while rare non-collapsed runs indicate potential signal that is difficult to use in isolation. (c) Full-token training implicitly averages over the spectrum. Entropy-aware soft reweighting is used as a validating intervention to test whether explicitly navigating this spectrum can combine anchor stability with explorer potential.

exchangeable. We ask not only whether a sparse token subset can estimate the full objective, but which structured subsets provide stable, complementary, or volatile signal.

This question matters because sequence-level metrics can hide very different token-level mechanisms. A run may look healthy while relying mostly on stable but narrow updates, or it may destabilize when broader signals are emphasized too early. Identifying which tokens supply reliable support and which tokens carry harder but more volatile signal is therefore useful both for diagnosis and for designing less brittle token allocation rules.

We study this question through *attention entropy*, a forward-pass diagnostic of how concentrated or diffuse a token’s contextual support is. Random 20% token subsets first show that token-level RL objectives are *sparsely estimable*; the main finding is that structured sparse subsets are not interchangeable. Attention entropy separates response tokens into an *optimization spectrum* with two poles:

- **Anchor tokens** (low attention entropy) rely on sparse selective support. They provide stable, well-aligned gradients and form a reliable optimization backbone, but anchor-only training tends to plateau on harder tasks.
- **Explorer tokens** (high attention entropy) aggregate diffuse multi-position context. Their gradients are strong but directionally volatile; explorer-only training usually collapses, yet non-collapsed trajectories suggest that these tokens can contain complementary hard-reasoning signal when optimization is stabilized.

This spectrum view reframes full-token training as an implicit average over heterogeneous token-level signals. We support it with evidence-gathering analyses, entropy dynamics, gradient geometry, and controls for position and next-token uncertainty, then use dynamic entropy-aware soft reweighting as a validating intervention rather than a tuned replacement for existing RL algorithms.

Our contributions:

- We introduce attention entropy as a token-level diagnostic for RL reasoning and use it to identify an optimization spectrum with stable anchor tokens and volatile explorer tokens as its two poles.
- We provide optimization-spectrum evidence through selective-training outcomes, support-concentration statistics, entropy dynamics, and gradient geometry.

- We use control subsets to test alternative explanations based on position and predictive entropy, with additional controls in the appendix.
- We validate the preceding analysis with a simple entropy-aware soft-reweighting intervention, improving the held-out average on Qwen3-8B-Base from 34.39 to 37.40 in the strongest entropy-source setting under the strict exact-match evaluation protocol; representative shallow, mid, and deep entropy sources all outperform full-token DAPO but exhibit different benchmark profiles.

2 Preliminaries and Training Setup

We study token-level training signals in RLVR using Qwen3 models optimized with VeRL and the DAPO objective. Unless otherwise stated, our controlled experiments use Qwen3-8B-Base, $n = 8$ rollouts per prompt, DeepScaler plus MATH level-3-to-5 prompts, and strict `\boxed{\}` answer matching for evaluation. Full implementation and evaluation details are provided in Appendix B. Let x denote the prompt and $y = (y_1, \dots, y_T)$ denote the generated response. Our analysis focuses on response tokens only.

We use two matched experiment families. Hard-masked selective training exposes the role of token subsets by updating only selected response tokens, while the full-data intervention replaces binary token selection with soft token weights so that all valid response tokens remain in the objective. Therefore, absolute scores are compared within a matched family.

Optimization uses a token-level objective:

$$\mathcal{L}_{\text{full}} = \frac{1}{T} \sum_{t=1}^T \ell_t, \quad (1)$$

where ℓ_t denotes the effective loss at token t .

Attention entropy. For response token y_t at captured layer ℓ , we average attention probabilities over all heads in that layer to obtain a layer-level attention distribution $a_{t,j}^{(\ell)}$ over visible positions j . We define:

$$H_t^{\text{raw}} = - \sum_{j=1}^{N_t} a_{t,j}^{(\ell)} \log a_{t,j}^{(\ell)}, \quad H_t^{\text{norm}} = \frac{H_t^{\text{raw}}}{\log N_t}. \quad (2)$$

The normalization removes the mechanical growth of raw entropy with visible context length. We use H_t^{norm} as the default metric and, unless the entropy-source layer is explicitly varied, compute it from one fixed mid-layer without cross-layer averaging. Details, variants, and layer-wise discussion are in Appendices D.1 and E. The fixed-layer choice is for controlled comparison rather than a claim of optimality; the main intervention table also reports representative shallow and deep entropy sources to show that the effect is not tied uniquely to Layer 20.

Token partition and naming. For each response, we rank tokens by entropy *within the same sample* and define:

- **Anchor tokens:** the bottom 20% by H_t^{norm} within each sample.
- **Explorer tokens:** the top 20% by H_t^{norm} within each sample.

This within-sample partition avoids comparing entropy magnitudes across responses of different lengths or difficulty levels. Details in Appendix D.2.

Weighted training objective. We study token subsets with:

$$\mathcal{L}_w = \frac{\sum_{t=1}^T w_t \ell_t}{\sum_{t=1}^T w_t}, \quad (3)$$

where $w_t \geq 0$. This unifies hard masking and random sparse training; the soft-reweighting intervention uses continuous advantage weights with all-token normalization (Appendix D.3).

Training configurations. We compare: (1) full-token training, (2) random-20% training, (3) anchor-only training (bottom 20% entropy), and (4) explorer-only training (top 20% entropy).

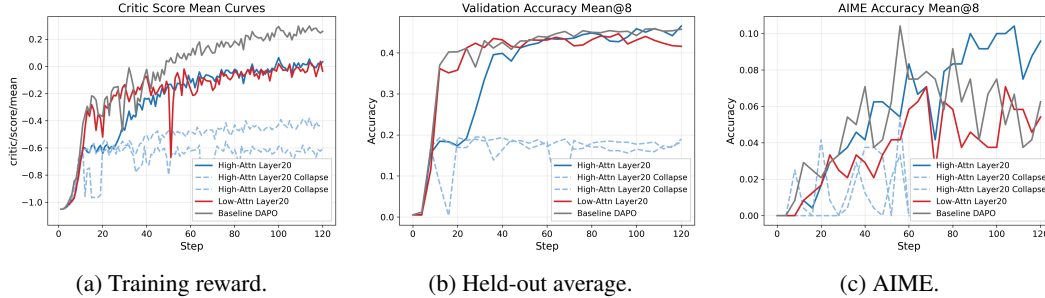


Figure 2: Entropy-based selective training reveals an optimization spectrum. Anchors provide stable but ceiling-limited updates; explorers are fragile in isolation, while rare non-collapsed runs expose hard-benchmark signal.

Control configurations. We compare against controls based on response position and next-token predictive entropy. Objective-magnitude, token-type, and matched-random controls are included as additional axes for the extended control analysis. Precise definitions are in Appendix F.

3 Selective Training Reveals an Optimization Spectrum

3.1 Sparse baseline and entropy-selected departures

Uniformly random 20% token training first establishes that the token-level RL objective is sparsely estimable. In the selective-training diagnostic setup, it reaches 42.60 final mean@8 accuracy versus 43.55 for matched full-token DAPO, recovering 97.8% of the full-token score; the last-five-checkpoint average gives the same conclusion (41.56 versus 43.09, or 96.4%). Appendix C gives the sparse-gradient derivation, and Appendix Figure 6 shows the trajectory. These numbers are used only within this diagnostic setup because the intervention experiments in Table 1 use a different dataset and step budget.

3.2 Anchors are stable; explorers are fragile but informative

Figure 2 shows that entropy-defined subsets are not interchangeable sparse estimators. Anchor-only training is stable and competitive on most held-out benchmarks, with no reward or length collapse, but it saturates earlier than full-token DAPO and lags most clearly on AIME. Anchors therefore act as a reliable optimization backbone rather than a complete substitute for all tokens.

Explorer-only training has the opposite profile. With the same 20% token budget, 5 of 8 independent runs collapse through short responses, length instability, or reasoning degeneration (Appendix G.3; Appendix Table 11). The 3 non-collapsed runs are thus a conditional diagnostic rather than a method comparison: they reach 12.31 ± 0.53 on AIME, 6.48 points above the matched full-token baseline (5.83 ± 0.89), and average 46.13 ± 1.58 on the other held-out benchmarks. The bimodality in Figure 14 indicates that explorers are not merely noise, but their useful signal is trajectory-sensitive and difficult to optimize without a stable backbone.

This asymmetry is the key empirical distinction. Anchors provide dependable updates but do not cover all reasoning-relevant signal; explorers can contain hard-benchmark signal, yet often destabilize optimization when used alone. We therefore treat successful explorer-only seeds as evidence about signal quality under stable trajectories, not as a competitive method. The intervention below aims to retain the anchor backbone while making explorer-like signal usable through softer allocation.

3.3 Spectrum summary and controls

Random-20% training falls between anchors and explorers because it samples across the spectrum without structural bias. Full-token training can therefore be viewed as an implicit average over stable anchor-like updates and broader, more volatile explorer-like updates. This also explains why hard masking is a diagnostic tool rather than a recommended training rule: anchor-only training loses coverage, while explorer-only training loses stability.

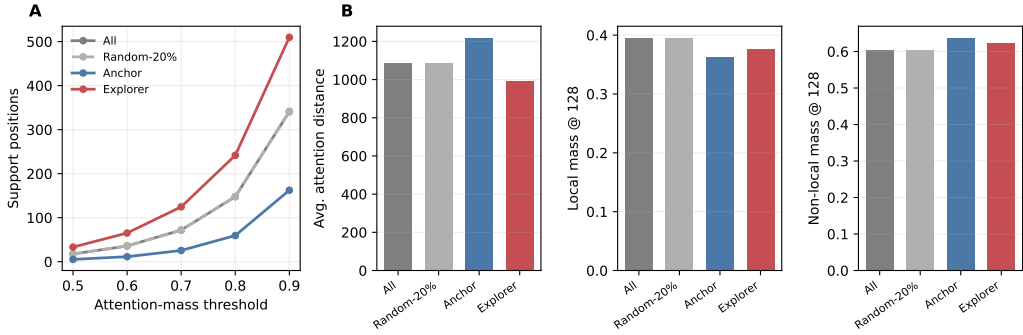


Figure 3: Evidence-gathering patterns under normalized attention entropy. Anchors require fewer support positions than explorers to accumulate the same attention mass; spatial-span statistics vary across entropy definitions, so support concentration is the stable interpretation.

The pattern is not explained by simpler token attributes. Normalization changes the severity but not the existence of explorer failure (Appendix G). Position controls fail to reproduce the entropy-defined behavior: front-only training largely fails, and back-only training remains weaker than full-token DAPO. Prediction entropy is also distinct from attention entropy, with only weak token-level correlation ($r = -0.1926$ over 97,995 response tokens) and qualitatively different off-diagonal token populations. Full control definitions and additional results are in Appendix F.

These controls rule out two shortcuts: entropy selection is not merely a position mask, and attention entropy is not next-token uncertainty under another name. A token can be uncertain but contextually selective, or confident but supported by diffuse evidence.

This distinction is important for interpreting the spectrum. Predictive entropy is about uncertainty over possible continuations, while attention entropy is about how the generated token gathers contextual support. The two quantities can therefore disagree on exactly the cases that matter for reasoning: a locally uncertain operation may rely on a small set of premises, whereas a predictable transition can still aggregate evidence from many positions.

4 Mechanistic Evidence for the Optimization Spectrum

Support concentration. Attention entropy organizes tokens by support concentration rather than locality. We measure how many positions are needed to accumulate a fixed attention-mass threshold, along with spatial-span statistics. Anchors concentrate mass on a small set of salient positions, nearby or distant; explorers spread mass across many positions. The causal relevance of this support structure is tested indirectly by selective training, controls, and gradient geometry.

This evidence-gathering view is useful because it gives the entropy groups a mechanistic interpretation beyond their scalar scores. Low-entropy tokens are not simply “easy” tokens; they are tokens whose current generation can be supported by a small effective set of context positions. High-entropy tokens are not simply “hard” tokens either; they are tokens whose update aggregates a broader support set and can therefore be more sensitive to which pieces of the reasoning trace are emphasized. This distinction is why we treat attention entropy as a support diagnostic rather than as a direct reward, difficulty, or importance estimator.

Figure 3 shows a consistent concentration separation: anchors rely on sparse selective support, whereas explorers aggregate diffuse multi-position support. Random-20% tokens track the all-token statistics, as expected. The concentration distinction persists under alternative entropy definitions, while distance-based statistics are less stable; additional variants and qualitative maps are in Appendix H.

Thus the stable axis is sparse-versus-diffuse support, not local-versus-global attention: under normalized entropy, anchors can even be slightly more non-local because they selectively retrieve a few salient positions from a long visible context.

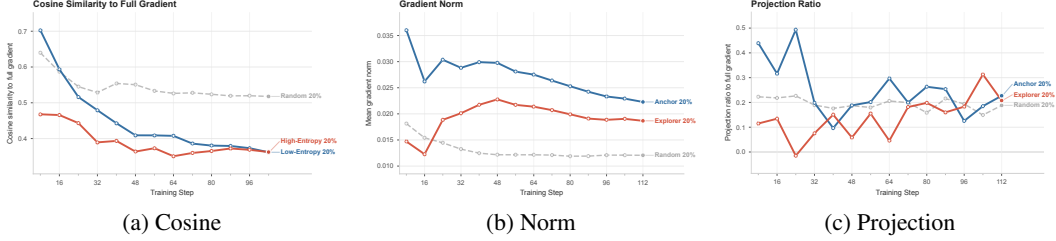


Figure 4: Gradient diagnostics against the full-token update. Random subsets are most aligned, anchors are aligned early but drift, and explorers have substantial norm but volatile direction and projection.

Entropy dynamics. Because anchors and explorers are defined by within-response entropy percentiles, their ordering is expected at each step; the relevant question is whether RL collapses the separation. It does not. Across Qwen3-14B and Qwen3-8B, Appendix Figure 20 shows explorers remaining in a high-entropy support regime, anchors remaining in a low-entropy regime, and full-token statistics between them even as means drift. Raw, top- k , and fixed-position variants show the same qualitative separation (Appendix I).

Together with selective-training results, these dynamics show that structurally distinct token groups persist during RL and remain optimization-relevant. Volatility is not inferred from entropy dispersion alone; it is established by explorer collapse and the gradient instability below.

This persistence is important for using entropy as a training coordinate. If the anchor/explorer distinction disappeared after a few updates, entropy-aware allocation would only be a transient initialization heuristic. Instead, the separation remains visible while the policy changes, so the current attention pattern can provide a coarse but repeatedly available signal about which tokens are supported by concentrated evidence and which require broader aggregation.

Gradient geometry. The same spectrum appears in update geometry. Let g_{full} be the full-token gradient and g_S the gradient from $S \in \{\text{anchor, explorer, rand}\}$. We compare:

$$\text{NormRatio}(S) = \frac{\|g_S\|_2}{\|g_{\text{full}}\|_2}, \quad (4)$$

$$\text{Cosine}(S) = \frac{\langle g_S, g_{\text{full}} \rangle}{\|g_S\|_2 \|g_{\text{full}}\|_2}, \quad (5)$$

$$\text{ProjRatio}(S) = \frac{\langle g_S, g_{\text{full}} \rangle}{\|g_{\text{full}}\|_2^2}. \quad (6)$$

Cosine measures directional agreement, norm ratio measures magnitude, and projection ratio measures effective contribution along the full-token update.

Figure 4 shows that the distinction is not simply gradient magnitude. Random subsets remain the closest sparse approximation to the full-token gradient. Anchor gradients are strongly aligned early (around 0.7 cosine similarity) but decline, matching stable training with a lower ceiling. Explorer gradients can be large, yet pass through a low-alignment middle phase and remain volatile in projection. Decile-level probes in Appendix J.1 show that useful update mass shifts across the entropy spectrum, motivating soft reweighting rather than fixed hard masking.

This reconciles anchor stability with explorer potential: high-entropy tokens can produce strong updates, but low cosine and volatile projection mean those updates are not consistently aligned with the full-token trajectory. Useful signal is distributed across entropy bands and changes over training, arguing against a fixed hard partition as the final training rule.

The gradient evidence also explains why random sparse subsets are a strong baseline. Random tokens approximate the full-token update because they sample the whole spectrum, but they do not expose which parts of the spectrum are stable, ceiling-limited, or volatile. Entropy-structured probes sacrifice some sparse-estimation optimality in order to reveal those roles.

Table 1: Qwen3-8B-Base results under the matched intervention setup. “Avg.” is the arithmetic mean over AIME, OlympiadBench, Minerva, and MATH. Reported \pm values summarize repeated runs under the same protocol; explorer successful seeds are a conditional diagnostic; the high-prediction-entropy row is a predictive-entropy control.

Method	AIME	OlympiadBench	Minerva	MATH	Avg.
Full-token DAPO	5.83 \pm 0.89	34.24 \pm 1.07	25.69 \pm 1.41	71.80 \pm 1.31	34.39 \pm 0.47
Random-20%	8.12 \pm 0.96	32.83 \pm 1.33	22.94 \pm 1.52	70.91 \pm 1.13	33.70 \pm 0.71
High Prediction Entropy-only	1.84 \pm 1.34	33.67 \pm 0.46	27.47 \pm 1.52	74.41 \pm 0.98	34.35 \pm 1.14
Anchor-only	5.60 \pm 0.77	30.47 \pm 0.96	24.39 \pm 0.88	66.43 \pm 1.04	31.72 \pm 0.43
Explorer-only, all seeds	4.62 \pm 5.96	20.18 \pm 13.18	16.82 \pm 4.60	46.79 \pm 18.80	22.10 \pm 10.64
Explorer-only, successful seeds (diagnostic)	12.31 \pm 0.43	37.18 \pm 0.99	22.73 \pm 0.66	70.98 \pm 1.21	35.80 \pm 0.82
Entropy reweighting, shallow layer (Layer 8)	7.37 \pm 1.18	36.95 \pm 1.10	31.41 \pm 1.39	73.88 \pm 1.49	37.40 \pm 0.81
Entropy reweighting, mid layer (Layer 20)	9.75 \pm 1.21	36.48 \pm 1.17	28.22 \pm 1.34	74.15 \pm 1.52	37.15 \pm 0.77
Entropy reweighting, deep layer (Layer 31)	9.14 \pm 1.19	37.86 \pm 1.24	28.86 \pm 1.28	73.54 \pm 1.44	37.35 \pm 0.78

5 Validation Intervention: Dynamic Entropy-Aware Soft Reweighting

Hard masks reveal the spectrum but are too extreme as a training rule: anchor-only training loses coverage and explorer-only training loses stability. We therefore use dynamic entropy-aware soft reweighting as a validation intervention. Each generated token receives a continuous advantage weight from normalized decision attention entropy, so all valid response tokens remain in the objective. The **Low2High** schedule emphasizes low-entropy tokens early and shifts weight toward high-entropy tokens during warmup, testing whether explorer-like signal becomes useful after a stable backbone forms. Details and controls are in Appendix K.

The intervention is deliberately simple. It does not introduce a new reward model, discard middle-spectrum tokens, or tune a benchmark-specific schedule. Its purpose is narrower: if attention entropy identifies actionable structure, then smoothly changing token weights along that spectrum should improve the matched training setup while preserving full-token coverage.

Low2High is also designed to match the empirical asymmetry rather than to privilege one endpoint permanently. Early low-entropy emphasis follows the selective-training evidence that anchors provide reliable directional support. Later high-entropy emphasis tests whether explorer-like updates become useful after the trajectory has accumulated enough stable structure. The reverse High2Low schedule is therefore a meaningful control: it uses the same endpoints and the same continuous weighting machinery, but exposes the volatile side of the spectrum before the anchor-like backbone has formed.

5.1 Empirical effect on Qwen3-8B-Base

Table 1 evaluates Qwen3-8B-Base under the matched VeRL-DAPO setup and strict boxed-answer exact-match protocol. Explorer successful seeds are shown only as the conditional diagnostic from Section 3; additional seed, layer-source, schedule, and model checks are in Appendix K.1– K.4.

Across entropy-source settings, entropy-aware reweighting improves over full-token DAPO on the held-out average and on every benchmark, but the layer source changes the gain profile. Shallow reaches the strongest average (37.40) and Minerva score; mid-layer is the original controlled setting and gives the strongest AIME and MATH among entropy rows; deep gives the strongest OlympiadBench. This supports actionable signal heterogeneity: different layers expose useful but non-identical allocation signals. The high-prediction-entropy control is a sharp contrast: it nearly matches full-token DAPO on average (34.35 versus 34.39) and is strongest on MATH (74.41), but drops AIME to 1.84, so next-token uncertainty does not recover the hard-reasoning allocation exposed by attention-support entropy.

We do not interpret the layer comparison as a full layer sweep or as evidence that one depth should be tuned as a benchmark knob. Rather, the shallow, mid, and deep rows test whether the diagnostic survives moving away from the original Layer-20 controlled setting. The answer is positive, but not uniform: a shallower source favors Minerva and the aggregate average, the mid-layer source keeps the strongest AIME and MATH results among entropy rows, and the final-layer source favors OlympiadBench. This pattern is consistent with different depths mixing local computation, evidence integration, and output-facing structure in different proportions. The shared result is that all three

Table 2: Schedule ablation for entropy-aware soft reweighting on Qwen3-8B-Base using the fixed Layer-20 entropy source. Static endpoint biases are weaker than dynamic temporal allocation. Low2High is the main Layer-20 schedule; High2Low is a reverse-order control.

Variant	Early	Late	AIME	OlympiadBench	Minerva	MATH	Avg.	Avg. w/o AIME
Full-token DAPO	uniform	uniform	5.83	34.24	25.69	71.80	34.39	43.91
Static anchor-biased	low	low	5.78	34.18	25.80	71.23	34.25	43.74
Static explorer-biased	high	high	5.59	33.97	25.88	77.60	35.76	45.82
Dynamic Low2High	low	high	9.75	36.48	28.22	74.15	37.15	46.28
Dynamic High2Low	high	low	3.78	38.84	29.58	75.18	36.85	47.87

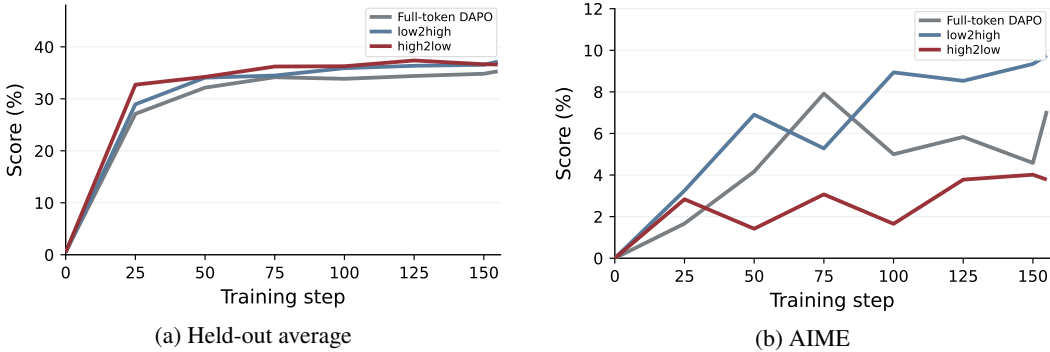


Figure 5: Training curves for the main Low2High schedule and reverse High2Low control. Both dynamic schedules improve the aggregate average, but Low2High gives a stronger late-stage AIME trajectory, consistent with stabilizing early training before increasing high-entropy emphasis.

entropy-source settings improve the held-out average over full-token DAPO while exposing different allocation profiles.

5.2 Robustness and schedule ablations

The seed-robustness and schedule ablations use the original fixed Layer-20 entropy source. Over three seeds, full-token DAPO obtains 34.39 ± 0.47 average accuracy, while Layer-20 entropy-aware reweighting obtains 37.15 ± 0.77 with benchmark-wise gains. The shallow- and deep-layer rows in Table 1 test entropy-source sensitivity.

Table 2 adds two qualifications. Fixed endpoint biases miss either coverage or stability: anchor bias is stable but does not improve the average, while explorer bias mainly helps MATH. Dynamic schedules are stronger, but order matters. High2Low is strong without AIME, whereas Low2High is much stronger on AIME and is the best Layer-20 schedule, consistent with stabilizing early before increasing exposure to volatile explorer-like signal.

This also clarifies the role of the hard masks used earlier. Anchor-only and explorer-only training are intentionally extreme probes: they separate stability from coverage by removing most tokens from the objective. The soft intervention keeps all valid response tokens and changes only their relative influence. It therefore tests whether attention entropy is actionable without turning the analysis into a brittle token-selection rule.

Figure 5 gives the trajectory view: High2Low rises quickly on average but remains weak on AIME, while Low2High behaves as a conservative allocation rule that begins with stable anchor-like updates and then increases explorer-like coverage. Additional transfer checks on Qwen3-14B and Qwen2.5-7B improve held-out average and AIME (Appendix K.4), suggesting that the effect is not isolated to Qwen3-8B-Base.

6 Related Work

RLVR and token-level credit. RLVR methods such as GRPO, DeepSeek-R1, and DAPO improve reasoning with verifiable outcome rewards [Shao et al., 2024, Guo et al., 2025, Yu et al., 2025], but

mostly optimize the response as a unit. Process-supervision and token-level reward work adds denser feedback [Lightman et al., 2023, Wang et al., 2024, Cui et al., 2025a, Zhong et al., 2025]. Our work is complementary: we analyze the native token-level objective induced by outcome-supervised RLVR. This distinction matters because no extra verifier, process label, or reward model is introduced. The same rollout-level reward is still used, but its token-level update terms are organized by an internal support diagnostic. The resulting question is therefore not whether additional supervision can identify better reasoning steps, but whether the policy’s own attention structure reveals which parts of an outcome-supervised update are stable, volatile, or coverage-limited.

Entropy and attention support. Recent RLVR analyses connect non-uniform token updates to next-token policy entropy or sparse critical positions [Cui et al., 2025b, Wang et al., 2025, He et al., 2026, Meng et al., 2026]. We instead study attention entropy, which measures contextual-support concentration rather than uncertainty over possible next tokens. Attention entropy has also been used to diagnose context utilization and information seeking [Zhang et al., 2025, Su et al., 2024]; we connect it to selective-training behavior, entropy dynamics, gradient alignment, and a validating reweighting intervention. Appendix A gives a fuller discussion.

Our layer-source analysis also differs from standard layer probing. We do not use shallow, middle, and final layers to claim a universal best depth, nor do we optimize the layer choice per benchmark. Instead, the comparison is a sensitivity check on whether attention entropy remains useful when computed from different representational depths. The observed shifts across AIME, OlympiadBench, Minerva, and MATH are useful because they expose different allocation profiles without changing the reward, data, optimizer, or evaluation protocol. This makes the main intervention closer to a diagnostic stress test than to a new architecture or benchmark-specific training recipe.

A second difference is the validation criterion. Token-importance analyses can remain correlational if they only rank positions or correlate scores with final answers. Our protocol first uses hard selective training to expose asymmetric failure modes, then checks support concentration and gradient alignment, and finally asks whether a soft reweighting rule improves the matched RLVR setup. This sequence is deliberately conservative: the diagnostic must explain behavior, survive controls, and support an intervention that keeps full response coverage. It also prevents the empirical claim from resting on successful explorer-only seeds, which remain conditional diagnostics rather than method comparisons. This matters for RLVR because optimization can fail through response-length collapse or unstable reasoning even when some high-entropy tokens contain useful benchmark signal.

7 Conclusion

We introduced attention entropy as a token-level diagnostic for RL reasoning and showed that it reveals an optimization spectrum. Low-entropy anchors provide stable but ceiling-limited updates, whereas high-entropy explorers use diffuse support and can carry complementary but volatile signal. Evidence-gathering statistics, entropy dynamics, gradient geometry, and position/prediction-entropy controls support this heterogeneous-signal view.

The main implication is that useful RL signal is distributed but not homogeneous. Hard masks expose the roles of different token groups, while dynamic entropy-aware soft reweighting shows that the diagnostic can improve token allocation without removing tokens from the objective. Attention entropy should therefore be read as a support-structure coordinate, not as a standalone token importance score.

Limitations. The results are a controlled case study on Qwen models with VeRL-DAPO, not a claim of universal transfer. We use one fixed mid-layer probe for the controlled mechanistic analyses, and the layer-source comparison checks only representative shallow, middle, and final layers. The schedule ablation also leaves open whether the allocation rule should adapt online to training dynamics. Our evidence is also at the level of entropy-defined token groups and allocation rules, rather than a head-by-head causal localization of attention behavior. Future work should separate which depth best exposes token-level support, when training should move from anchor-like stability to explorer-like coverage, and whether allocation can react to collapse indicators such as response length, reward stagnation, or gradient misalignment.

References

- Ganqu Cui, Lifan Yuan, Zefan Wang, Hanbin Wang, Wendi Li, Bingxiang He, Yuchen Fan, Tianyu Yu, Qixin Xu, Weize Chen, Jiarui Yuan, Huayu Chen, Kaiyan Zhang, Xingtai Lv, Shuo Wang, Yuan Yao, Xu Han, Hao Peng, Yu Cheng, Zhiyuan Liu, Maosong Sun, Bowen Zhou, and Ning Ding. Process reinforcement through implicit rewards. *arXiv preprint arXiv:2502.01456*, 2025a.
- Ganqu Cui, Yuchen Zhang, Jiacheng Chen, Lifan Yuan, Zhi Wang, Yuxin Zuo, Haozhan Li, Yuchen Fan, Huayu Chen, Weize Chen, Zhiyuan Liu, Hao Peng, Lei Bai, Wanli Ouyang, Yu Cheng, Bowen Zhou, and Ning Ding. The entropy mechanism of reinforcement learning for reasoning language models. *arXiv preprint arXiv:2505.22617*, 2025b.
- Daya Guo, Dejian Yang, Haowei Zhang, Junxiao Song, Ruoyu Zhang, Runxin Xu, Qihao Zhu, Shirong Ma, Peiyi Wang, Xiao Bi, et al. DeepSeek-R1: Incentivizing reasoning capability in LLMs via reinforcement learning. *arXiv preprint arXiv:2501.12948*, 2025.
- Chaoqun He, Renjie Luo, Yuzhuo Bai, Shengding Hu, Zhen Thai, Junhao Shen, Jinyi Hu, Xu Han, Yujie Huang, Yuxiang Zhang, et al. Olympiadbench: A challenging benchmark for promoting agi with olympiad-level bilingual multimodal scientific problems. In *Proceedings of the 62nd Annual Meeting of the Association for Computational Linguistics (Volume 1: Long Papers)*, pages 3828–3850, 2024.
- Yuhang He, Haodong Wu, Siyi Liu, Hongyu Ge, Hange Zhou, Keyi Wu, Zhuo Zheng, Qihong Lin, Zixin Zhong, and Yongqi Zhang. Rethinking token-level credit assignment in RLVR: A polarity-entropy analysis. *arXiv preprint arXiv:2604.11056*, 2026.
- Dan Hendrycks, Collin Burns, Saurav Kadavath, Akul Arora, Steven Basart, Eric Tang, Dawn Song, and Jacob Steinhardt. Measuring mathematical problem solving with the math dataset. *arXiv preprint arXiv:2103.03874*, 2021.
- Aitor Lewkowycz, Anders Andreassen, David Dohan, Ethan Dyer, Henryk Michalewski, Vinay Ramasesh, Ambrose Slone, Cem Anil, Imanol Schlag, Theo Gutman-Solo, et al. Solving quantitative reasoning problems with language models. *Advances in neural information processing systems*, 35:3843–3857, 2022.
- Hunter Lightman, Vineet Kosaraju, Yuri Burda, Harrison Edwards, Bowen Baker, Teddy Lee, Jan Leike, John Schulman, Ilya Sutskever, and Karl Cobbe. Let’s verify step by step. In *The twelfth international conference on learning representations*, 2023.
- Michael Luo, Sijun Tan, Justin Wong, Xiaoxiang Shi, William Y Tang, Manan Roongta, Colin Cai, Jeffrey Luo, Tianjun Zhang, Li Erran Li, et al. Deepscaler: Surpassing o1-preview with a 1.5 b model by scaling rl. *Notion Blog*, 3(5), 2025.
- Haoming Meng, Kexin Huang, Shaohang Wei, Chiyu Ma, Shuo Yang, Xue Wang, Guoyin Wang, Bolin Ding, and Jingren Zhou. Sparse but critical: A token-level analysis of distributional shifts in RLVR fine-tuning of LLMs. *arXiv preprint arXiv:2603.22446*, 2026.
- Zhihong Shao, Peiyi Wang, Qihao Zhu, Runxin Xu, Junxiao Song, Xiao Bi, Haowei Zhang, Mingchuan Zhang, Y. K. Li, Y. Wu, and Daya Guo. DeepSeekMath: Pushing the limits of mathematical reasoning in open language models. *arXiv preprint arXiv:2402.03300*, 2024.
- Weihang Su, Yichen Tang, Qingyao Ai, Zhijing Wu, and Yiqun Liu. DRAGIN: Dynamic retrieval augmented generation based on the real-time information needs of large language models. In *Proceedings of the 62nd Annual Meeting of the Association for Computational Linguistics (Volume 1: Long Papers)*, pages 12991–13013, Bangkok, Thailand, 2024. Association for Computational Linguistics. doi: 10.18653/v1/2024.acl-long.702. URL <https://aclanthology.org/2024.acl-long.702/>.
- Peiyi Wang, Lei Li, Zhihong Shao, Runxin Xu, Damai Dai, Yifei Li, Deli Chen, Yu Wu, and Zhifang Sui. Math-shepherd: Verify and reinforce LLMs step-by-step without human annotations. In *Proceedings of the 62nd Annual Meeting of the Association for Computational Linguistics (Volume 1: Long Papers)*, pages 9426–9439, Bangkok, Thailand, 2024. Association for Computational Linguistics. doi: 10.18653/v1/2024.acl-long.510. URL <https://aclanthology.org/2024.acl-long.510/>.

- Shenzhi Wang, Le Yu, Chang Gao, Chujie Zheng, Shixuan Liu, Rui Lu, Kai Dang, Xionghui Chen, Jianxin Yang, Zhenru Zhang, Yuqiong Liu, An Yang, Andrew Zhao, Yang Yue, Shiji Song, Bowen Yu, Gao Huang, and Junyang Lin. Beyond the 80/20 rule: High-entropy minority tokens drive effective reinforcement learning for LLM reasoning. *arXiv preprint arXiv:2506.01939*, 2025.
- Qiyong Yu, Zheng Zhang, Ruofei Zhu, Yufeng Yuan, Xiaochen Zuo, Yu Yue, Weinan Dai, Tiantian Fan, Gaohong Liu, Lingjun Liu, et al. DAPO: An open-source LLM reinforcement learning system at scale. *arXiv preprint arXiv:2503.14476*, 2025.
- Zhisong Zhang, Yan Wang, Xinting Huang, Tianqing Fang, Hongming Zhang, Chenlong Deng, Shuaiyi Li, and Dong Yu. Attention entropy is a key factor: An analysis of parallel context encoding with full-attention-based pre-trained language models. In *Proceedings of the 63rd Annual Meeting of the Association for Computational Linguistics (Volume 1: Long Papers)*, pages 9840–9855, Vienna, Austria, 2025. Association for Computational Linguistics. doi: 10.18653/v1/2025.acl-long.485. URL <https://aclanthology.org/2025.acl-long.485/>.
- Han Zhong, Zikang Shan, Guhao Feng, Wei Xiong, Xinle Cheng, Li Zhao, Di He, Jiang Bian, and Liwei Wang. DPO meets PPO: Reinforced token optimization for RLHF. In *Proceedings of the 42nd International Conference on Machine Learning*, volume 267 of *Proceedings of Machine Learning Research*, pages 78498–78521. PMLR, 2025. URL <https://proceedings.mlr.press/v267/>.

A Detailed Related Work

RLVR for reasoning language models. Reinforcement learning with verifiable rewards (RLVR) has recently become a central approach for improving the reasoning ability of large language models. DeepSeekMath introduced Group Relative Policy Optimization (GRPO), which removes the value model in PPO-style training and estimates advantages from groups of sampled responses [Shao et al., 2024]. DeepSeek-R1 further demonstrated that large-scale RL can elicit long-chain reasoning behaviors from base models using verifiable outcome rewards [Guo et al., 2025]. Subsequent systems such as DAPO improved the reproducibility and scalability of RL reasoning training through practical algorithmic choices including decoupled clipping and dynamic sampling [Yu et al., 2025]. While these works establish RLVR as an effective training paradigm, they mainly operate at the sequence or response level. In contrast, our work studies the token-level structure of RLVR updates: rather than asking whether RLVR improves reasoning, we ask which response tokens provide stable or unstable learning signals during RL training.

Process rewards and token-level credit assignment. A major challenge in RLVR is that sparse outcome rewards must be assigned to many intermediate reasoning tokens. Prior work addresses this issue by introducing denser supervision. Process supervision and process reward models provide feedback for intermediate reasoning steps and can improve mathematical reasoning reliability [Lightman et al., 2023, Wang et al., 2024]. PRIME further explores implicit process rewards, deriving dense token-level reward signals from outcome labels and policy rollouts without requiring explicit human process annotations [Cui et al., 2025a]. Other work formulates alignment and preference optimization from a token-level perspective, learning token-wise reward or value signals for more fine-grained policy optimization [Zhong et al., 2025]. These methods aim to construct better token-level rewards. Our work is complementary: we do not introduce an external process reward model, but instead analyze the native token-level objective already used in RLVR and show that its learning signals are structurally heterogeneous.

Entropy-aware analyses of RLVR. Several recent works analyze RLVR through the lens of policy entropy. The Entropy Mechanism of Reinforcement Learning for Reasoning Language Models studies entropy collapse during RL reasoning training and argues that the exhaustion of policy entropy limits continued exploration [Cui et al., 2025b]. Beyond the 80/20 Rule shows that a small fraction of high-policy-entropy tokens act as reasoning forks and can dominate the effectiveness of RLVR updates [Wang et al., 2025]. Related work further connects token entropy to credit assignment, arguing that high-entropy positions carry more potential credit under outcome-supervised RLVR [He et al., 2026], and shows that RLVR induces sparse but critical token-level distributional shifts [Meng et al., 2026]. These studies reveal that RLVR updates are not uniformly distributed across tokens. However, they primarily define entropy over the next-token output distribution, measuring uncertainty over possible token choices. Our work studies a different internal signal: attention entropy. Instead of measuring how uncertain the model is about the next token, attention entropy measures how concentrated or diffuse a token’s contextual support is. This distinction allows us to identify anchor tokens with sparse selective support and explorer tokens with diffuse multi-position aggregation.

Attention entropy and internal support structure. Attention entropy has also been used as a diagnostic for how language models use context. Prior studies show that abnormal attention entropy can reveal failures in context encoding and that attention-based signals can expose a model’s information needs during generation [Zhang et al., 2025, Su et al., 2024]. These works suggest that attention entropy is a useful internal indicator of context utilization. We extend this perspective to RL reasoning training by connecting attention support structure with selective training behavior, entropy dynamics, and gradient geometry in RLVR.

B Experimental Details and Hyperparameters

This appendix provides the implementation details for the RLVR training experiments. The paper contains two matched experiment families: an earlier selective-training diagnostic setup and the full-data soft-reweighting intervention setup. Within each family, compared variants use the same base model, reward function, rollout configuration, data split, and step budget; the main intended

difference is the token-weighting rule applied to the response-token loss. Across families, however, the data and step budgets differ, so absolute scores should not be compared across tables.

B.1 Experiment-family summary

Table 3 summarizes the experiment families used in the paper. The selective-training experiments are validation-oriented diagnostics: to make the initial comparisons faster, they use 40% of the full training set, a different training-step budget, and validation subsets sampled from the full benchmark test sets. These validation subsets can be biased relative to the full test sets. We therefore interpret the selective training results only through comparisons against their matched full-token baseline, not as absolute scores comparable to the full-data intervention table.

Table 3: Summary of experiment families and comparability.

Experiment family	Purpose	Training data and steps	Evaluation data	Intended comparison
Selective-training diagnostic	Validate sparse estimability and expose anchor/explorer behavior	40% of the full training set; diagnostic step budget different from the full-data intervention setup	Subsets sampled from the full AIME, OlympiadBench, Minerva, and MATH test sets; potentially biased relative to the full test sets	Compare full-token, random-20%, anchor-only, and explorer-only runs within this matched diagnostic setup only
Soft-reweighting intervention	Test whether attention-entropy structure can inform token allocation	Full training set and the intervention step budget used for Table 1	Full benchmark evaluation used in Table 1	Compare the intervention against baselines in the same table; do not compare absolute scores to the diagnostic setup
Additional-model transfer checks	Supporting evidence for soft-reweighting intervention	ev- Same protocol family as the full-data intervention setup, applied to additional Qwen model settings	Same evaluation protocol as the intervention setup	Supporting transfer checks, not a universal effectiveness claim

B.2 Model, framework, and systems setup

All main experiments use the official Qwen3-8B-Base checkpoint with the original Qwen tokenizer. We train the model using VeRL with the original DAPO recipe. Training is performed in bf16 precision with FSDP. We enable gradient checkpointing, remove padding during model execution, and use dynamic batch sizing for actor, reference, and rollout log-probability computation. Unless otherwise specified, filter-group sampling is disabled to make selective-token training directly comparable with the full-token baseline.

B.3 Training and validation data

For the full-data intervention setup, we train on verifiable mathematical-reasoning prompts from DeepScaler(Luo et al. [2025]) and MATH(Hendrycks et al. [2021]) data. In our implementation, these correspond to the DeepScaler training split and the SimpleRL/Qwen training split. The selective-training diagnostic setup uses 40% of this full training pool and evaluates on subsets sampled from the full benchmark test sets, as summarized in Table 3. We do not apply additional data filtering. Prompts are read from the prompt field, and prompts exceeding the maximum prompt length are left-truncated.

Table 4: Model and systems configuration.

Item	Setting
Base model	Official Qwen3-8B-Base checkpoint
Tokenizer	Original Qwen tokenizer
RL framework	VeRL with the original DAPO recipe
Precision	bf16
Distributed training	FSDP
Gradient checkpointing	Enabled
Remove padding	Enabled
Dynamic batch size	Enabled for actor, reference, and rollout log-probability computation
Parameter offload	Enabled
Optimizer offload	Enabled
Tensor model parallel size	1
Sequence parallel size	1
GPUs	2 nodes for selective-training probes; 4 nodes for full-data intervention runs; 8 NVIDIA H800 80GB GPUs per node
Filter groups	Disabled

Table 5: Full-data intervention configuration.

Item	Setting
Training data	DeepScaler train split + MATH train split
Validation data	AIME + OLYMPIAD_BENCH He et al. [2024] + MINERVA Lewkowycz et al. [2022] + MATH test split
Prompt field	prompt
Data filtering	None
Prompt truncation	Left truncation
Maximum prompt length	1024
Maximum response length	8192
Maximum sequence length	9216

B.4 Reward function and overlong penalty

We use the DAPO reward manager with a rule-based verifier. For each generated response, we extract the content inside `\boxed{}` and compare it with the reference answer using string matching. The reward takes three values: -2 if no boxed answer is found, -1 if a boxed answer is found but does not match the reference answer, and 1 if the boxed answer is correct. All runs use the same overlong-response penalty.

Table 6: Reward configuration.

Item	Setting
Reward manager	DAPO
Answer extraction	Content inside <code>\boxed{}</code>
Verifier	String matching against the reference answer
Reward for missing boxed answer	-2
Reward for incorrect boxed answer	-1
Reward for correct boxed answer	1
Overlong buffer	Enabled
Overlong buffer length	2048
Overlong penalty factor	1.0

B.5 RL optimization hyperparameters

We use the GRPO-style advantage estimator in DAPO. We disable KL penalties both in the reward and in the actor loss in the main experiments, so the reference model is used for log-probability

computation but not for an explicit KL penalty. The actor entropy coefficient is set to zero. All selective-training variants use the same optimizer, clipping, and batch-size settings.

Table 7: RL optimization hyperparameters.

Item	Setting
Advantage estimator	GRPO
Use KL in reward	False
KL coefficient in reward	0.0
Use actor KL loss	False
Actor KL loss coefficient	0.0
Clip ratio low	0.2
Clip ratio high	0.28
Clip ratio constant c	10.0
Actor entropy coefficient	0.0
Optimizer	AdamW
Learning rate	1×10^{-6}
Warmup steps	10
Weight decay	0.1
Gradient clipping	1.0
Loss aggregation mode	Token mean
Training prompt batch size	512
Generation prompt batch size	1536
PPO mini-batch size	32
PPO micro-batch size	Dynamic / unset
Total epochs	10
Validation before training	True
Validation frequency	Every 4 training steps

B.6 Rollout and evaluation configuration

During training, each prompt is expanded into multiple sampled responses. The rollout temperature is set to 1.0, with top- $p = 0.95$ and no top- k truncation. For validation, we also use temperature 1.0 but set top- $p = 0.7$ to reduce evaluation variance. We sample 8 responses per validation prompt and report mean@8 unless otherwise specified.

Table 8: Rollout and evaluation configuration.

Item	Setting
Training responses per prompt	8
Training temperature	1.0
Training top- p	0.95
Training top- k	-1
Validation responses per prompt	8
Validation temperature	1.0
Validation top- p	0.7
Validation top- k	-1
Validation sampling	Enabled
Reported validation metric	mean@8

Metric definition. For each validation problem, we sample 8 responses and compute the fraction of correct responses under the same boxed-answer verifier. We report mean@8, i.e., the average correctness over the 8 sampled responses and then over all problems in the benchmark. This differs from majority voting or pass@8.

B.7 Attention-entropy instrumentation

For each response token, we compute attention entropy from the actor model during training. We use one fixed mid-layer attention probe and normalized attention entropy as the default score. Within the

captured layer, we average attention probabilities over all heads before computing entropy, yielding one layer-level attention distribution per response token. We do not average entropy across multiple layers in the main experiments. Attention entropy is used only to construct token weights or diagnostic statistics; it is detached from the optimization graph and is not used as an auxiliary loss.

Table 9: Attention-entropy configuration.

Item	Setting
Enable attention entropy	True
Captured layer	One fixed mid-layer probe (Layer 20 in our implementation)
Head aggregation	Average attention probabilities over all heads in the captured layer
Layer aggregation	None in main experiments; the layer is fixed before comparison within each setup
Default entropy score	Normalized attention entropy
Use normalized entropy	True
Store full attention probabilities	False
Compute attention entropy on CPU	False
Entropy variants	Normalized, raw, top- k , and fixed-window variants when enabled
Token entropy log frequency	Every 2 steps
Logged sequences per step	3
Maximum logged tokens per sequence	256
Entropy-detail save frequency	Every 2 steps
Support-size thresholds	0.5, 0.7, 0.9

For response token y_t , the entropy score is computed over visible positions under the causal attention mask. The token partition is performed within each generated response: anchor tokens are the bottom 20% by normalized attention entropy, and explorer tokens are the top 20%. The entropy scores are recomputed from the current rollout batch rather than fixed in advance.

B.8 Token-weighting configurations

All training variants optimize the same token-level RL objective but differ in the response-token weights w_t . Full-token training uses all valid response tokens. Random-sparse training samples a uniformly random 20% subset of response tokens. Anchor-only and explorer-only training select the bottom and top 20% tokens by normalized attention entropy within each response, respectively.

For the soft-reweighting validation intervention, we use attention entropy to assign continuous advantage weights instead of binary masks. The implementation uses the decision attention entropy for each generated token, applies a temperature-scaled softmax over valid response tokens in the rollout batch, min-max rescales the softmax scores, and maps them to scheduled low-entropy and high-entropy endpoint weights. The main controlled schedule is Low2High: the low-entropy endpoint is scheduled from 1.0 to 0.0, and the high-entropy endpoint is scheduled from 0.0 to 1.0. All valid response tokens receive continuous entropy-dependent weights rather than being split into a fixed middle band and endpoint groups.

Table 10: Token-weighting and reweighting configuration.

Setting	Token selection / weight	Normalization
Full-token	$w_t = 1$ for all valid response tokens	Token mean
Random-20%	Uniform Bernoulli mask with 20% budget	Selected-token or control-specific
Anchor-only	Bottom 20% by normalized attention entropy	Selected-token normalization
Explorer-only	Top 20% by normalized attention entropy	Selected-token normalization
Soft intervention	Continuous entropy-based advantage weights	All-token-weighted normalization

Normalization variants. For hard-masked selective training, the main normalization uses the selected tokens as the denominator, preserving the per-token loss scale of the retained tokens. For normalization controls and the smooth soft-reweighting intervention, we use all-token-weighted

normalization:

$$\mathcal{L}_w^{\text{all}} = \frac{1}{T} \sum_{t=1}^T w_t \ell_t, \quad (7)$$

where T is the number of valid response tokens. This variant keeps the response-level loss scale comparable across different weighting rules. We report normalization-specific results separately when they are used.

B.9 Control configurations

To test whether the anchor–explorer distinction is explained by simpler token properties, we additionally evaluate control masks. Position controls select the first or last 20% of response tokens. Prediction-entropy controls select tokens by next-token predictive entropy. Objective-magnitude controls select tokens by the magnitude of their effective loss contribution. Type-matched and position-matched random controls preserve coarse token-type or relative-position statistics while removing the attention-entropy ranking. These controls are defined in detail in Appendix F.

B.10 Compute Resources

All experiments were conducted on an internal GPU cluster. Each node contains 8 GPUs, so the 2-node and 4-node settings correspond to 16 and 32 GPUs per run, respectively. The GPUs used in our experiments were NVIDIA H800 with 80GB memory.

For the full-data soft-reweighting intervention experiments, including the matched full-token baselines and schedule/layer-source variants, each run used 4 nodes, i.e., 32 GPUs, and took approximately 18 wall-clock hours. This corresponds to roughly $32 \times 18 = 576$ GPU-hours per run. For the selective-training probe experiments on the smaller diagnostic data split, each run used 2 nodes, i.e., 16 GPUs, and took approximately 22 wall-clock hours, corresponding to roughly $16 \times 22 = 352$ GPU-hours per run.

Across the reported intervention runs, probe runs, multi-seed diagnostics, schedule ablations, and failed or preliminary runs used to diagnose instability, we estimate the total compute to be on the order of 1×10^4 – 2×10^4 GPU-hours. This estimate is intended to characterize the scale of compute required to reproduce the experimental study; small post-processing jobs for plotting, metric aggregation, and visualization are excluded.

B.11 Implementation details omitted from the paper

We omit machine-specific paths, proxy settings, process-management commands, and logging credentials from the paper and released configuration. These details do not affect the algorithmic setup or the reported results.

C Sparse Estimability Derivation

Let $g_t = \nabla_{\theta} \ell_t$ denote the per-token gradient and $g_{\text{full}} = \frac{1}{T} \sum_{t=1}^T g_t$. Under uniform random subsampling with inclusion probability p , each token is selected by $m_t \sim \text{Bernoulli}(p)$ and the subset gradient is $g_{\text{rand}} = \frac{1}{\sum_t m_t} \sum_t m_t g_t$ when the subset is non-empty. Conditional on a fixed subset size, this estimator is unbiased by symmetry. For large T , $\sum_t m_t$ concentrates near pT , yielding the approximation

$$\mathbb{E}[g_{\text{rand}}] \approx g_{\text{full}}, \quad (8)$$

$$\mathbb{E} \|g_{\text{rand}} - g_{\text{full}}\|^2 \approx \frac{1-p}{pT} \cdot \bar{V}, \quad (9)$$

where $\bar{V} = \frac{1}{T} \sum_t \|g_t\|^2$. The expected directional agreement can be approximated as

$$\mathbb{E} [\text{Cosine}(g_{\text{rand}}, g_{\text{full}})] \approx \frac{1}{\sqrt{1 + (1-p)\bar{V}/(pT\|g_{\text{full}}\|^2)}}. \quad (10)$$

This argument treats token gradients as fixed while analyzing mask randomness and does not apply to structured subsets, whose inclusion probabilities depend on token properties.

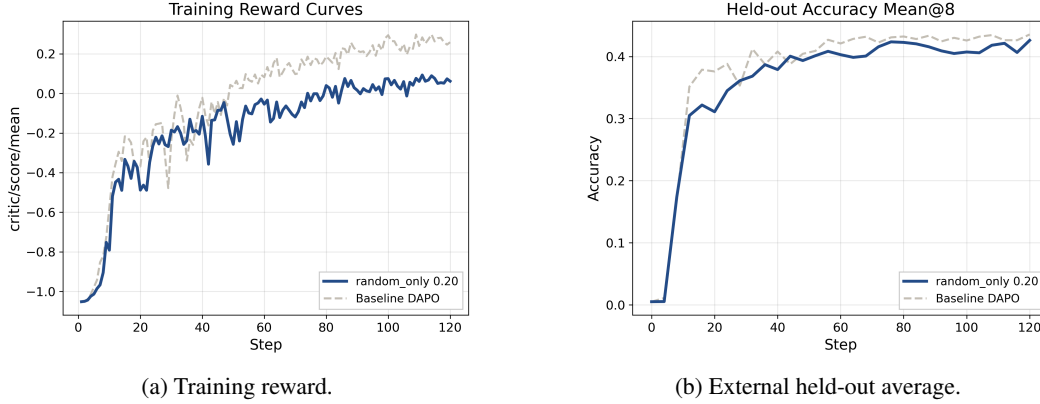


Figure 6: Token-level RL objectives are sparsely estimable. (a) On training-side reward, random-20% token training (gray) lags behind full-token training (black), reflecting residual variance from sparse gradient estimation. (b) On external held-out benchmarks, random-20% training recovers much of full-token performance.

D Additional Entropy Definitions and Implementation Details

D.1 Additional Attention Entropy Variants

In the main paper, we use normalized attention entropy as the default score. Here we provide additional variants used in robustness analyses. For response token y_t at layer ℓ , let $a_{t,j}^{(\ell)}$ denote the layer-level attention probability assigned to visible position j after averaging attention probabilities over all heads in that layer, with

$$\sum_{j=1}^{N_t} a_{t,j}^{(\ell)} = 1. \quad (11)$$

Raw attention entropy.

$$H_t^{\text{raw}} = - \sum_{j=1}^{N_t} a_{t,j}^{(\ell)} \log a_{t,j}^{(\ell)}. \quad (12)$$

Normalized attention entropy.

$$H_t^{\text{norm}} = \frac{H_t^{\text{raw}}}{\log N_t}. \quad (13)$$

Top- k attention entropy. Select the k largest attention weights, renormalize, and compute entropy:

$$\tilde{a}_{t,j}^{(k)} = \frac{a_{t,j}^{(\ell)}}{\sum_{j' \in S_k(t)} a_{t,j'}^{(\ell)}}, \quad H_t^{\text{top-}k} = - \sum_{j \in S_k(t)} \tilde{a}_{t,j}^{(k)} \log \tilde{a}_{t,j}^{(k)}. \quad (14)$$

Fixed-position attention entropy. Restrict to first $K = 256$ visible positions and renormalize:

$$\hat{a}_{t,j}^{(K)} = \frac{a_{t,j}^{(\ell)}}{\sum_{j' \in F_K(t)} a_{t,j'}^{(\ell)}}, \quad H_t^{\text{fix-}K} = - \sum_{j \in F_K(t)} \hat{a}_{t,j}^{(K)} \log \hat{a}_{t,j}^{(K)}. \quad (15)$$

Unless otherwise specified, analyses use the same fixed mid-layer probe across compared variants. Appendix E discusses the scope of this implementation choice and layer-wise follow-up diagnostics.

D.2 Entropy-based Token Partition

For each response, we compute H_t^{norm} for response tokens only and rank within-sample. Given threshold p :

$$\mathcal{T}_{\text{explorer}}^{(p)}(y) = \text{Top-}p\%(\mathcal{T}(y); H_t^{\text{norm}}), \quad \mathcal{T}_{\text{anchor}}^{(p)}(y) = \text{Bottom-}p\%(\mathcal{T}(y); H_t^{\text{norm}}). \quad (16)$$

We use $p = 20\%$ throughout. The within-sample partition focuses on relative functional role rather than absolute entropy magnitude.

D.3 Token Weighting and Normalization Details

For hard token masks, the weighted objective

$$\mathcal{L}_w = \frac{\sum_{t=1}^T w_t \ell_t}{\sum_{t=1}^T w_t} \quad (17)$$

normalizes by weight sum rather than total token count, avoiding gradient shrinkage when only a small subset is selected.

Hard mask. $w_t \in \{0, 1\}$.

Random sparse mask. $w_t \sim \text{Bernoulli}(p)$ with $p = 0.2$.

Smooth soft reweighting. The intervention in Section 5 uses continuous weights $w_t \in \mathbb{R}_{\geq 0}$ to rescale token-level advantages, but keeps the actor-loss denominator equal to the number of valid response tokens. This all-token-weighted normalization is used to avoid changing the denominator when the scheduled endpoint weights change.

E Layer-Wise Attention Patterns and Scope of the Fixed-Layer Probe

The main analysis uses attention entropy from one fixed mid-layer probe. This is an implementation choice made to keep all compared variants matched, not a claim that this layer is uniquely optimal or that all transformer layers expose the same token partition. Different layers can play different roles during reasoning generation. Earlier layers often retain more local lexical, syntactic, and positional regularities; middle layers are more likely to mix local computation with task-level state tracking; later layers can become more specialized toward generation decisions, output format, and answer expression. Because attention entropy measures the concentration of contextual support inside a particular layer, its numerical value and the resulting anchor/explorer partition may vary across layers.

This layer dependence is a feature of the diagnostic rather than a contradiction of the main results. The paper uses attention entropy to expose token-level heterogeneity in a controlled setting, not to claim that a single layer captures all forms of reasoning support. The fixed-layer probe provides one consistent view of support concentration that can be connected to selective training, support-size statistics, entropy dynamics, and gradient geometry. A full layer-wise intervention sweep is left for future work.

Several lightweight follow-up checks can be run before a full intervention sweep. First, one can compute anchor/explorer mask agreement across a small set of early, middle, and late layers using Jaccard overlap or rank correlation of token entropies within each response. Low agreement would show that different layers identify different support regimes, while high agreement around neighboring middle layers would support the stability of the fixed-layer probe. Second, the evidence-gathering statistics in Section 4 can be recomputed per layer: support-size thresholds, average attention distance, local-window mass, and non-local mass are inexpensive diagnostics once attention probabilities have been logged. Third, one can run the gradient-geometry probe from Section 4 with masks produced by neighboring layers. This is cheaper than full RL training and directly tests whether the directional-alignment patterns are specific to the chosen probe layer or stable across nearby layers. These checks would clarify which aspects of attention entropy are layer-specific and which are robust properties of token-level RL signal heterogeneity.

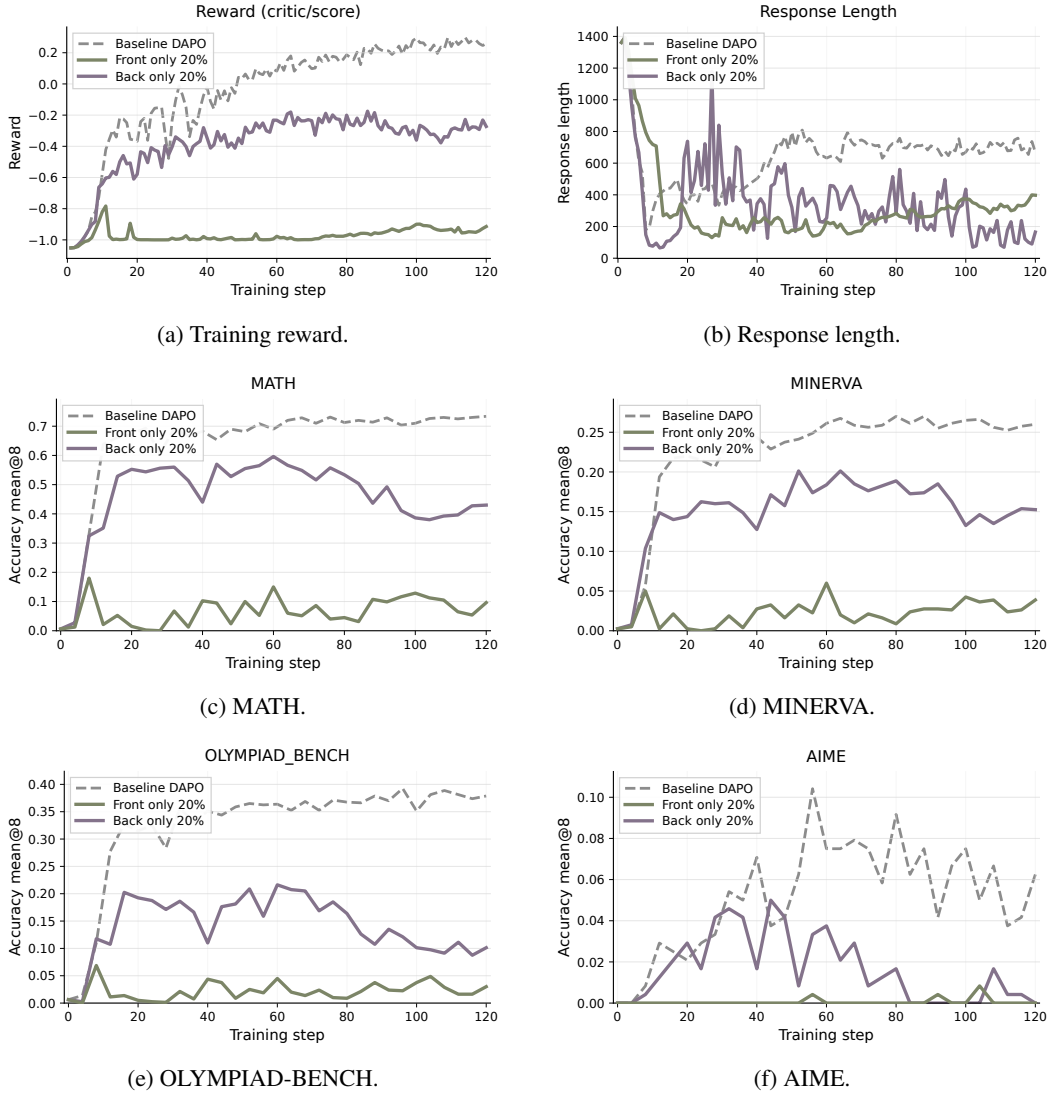


Figure 7: Position-only controls on Qwen3-8B-Base. These controls test whether attention entropy is merely a proxy for response position. We compare full-token DAPO with training only the first 20% or the last 20% response tokens. Front-only training largely fails, suggesting that early response tokens alone cannot support effective RLVR optimization. Back-only training is stronger, consistent with answer-proximal tokens carrying more direct outcome-relevant signal, but it remains substantially below full-token DAPO and shows late-stage degradation on harder benchmarks. The failure of fixed-position masks to reproduce the entropy-based behavior indicates that attention entropy captures more than token position.

F Alternative-Explanation Control Configurations

This section defines the control masks used to test whether the optimization roles of attention-entropy-defined token groups can be explained by simpler token properties. We focus on three alternative explanations: token position, prediction uncertainty, and token-level objective magnitude. All controls use the same 20% sparsity ratio as the anchor/explorer masks and are computed within each response unless otherwise specified.

F.1 Position Controls

A key possible confound is that attention entropy may be a proxy for token position. For example, low-entropy or high-entropy tokens might appear more frequently in certain regions of the response, in which case entropy-based selection could be explained by a simpler beginning-versus-end-of-response effect. To test this alternative explanation, we construct position-only controls that ignore attention entropy entirely.

For a response of length T , we define two fixed-position masks:

$$\mathcal{T}_{\text{front}}^{20\%} = \{t : t/T \leq 0.2\}, \quad \mathcal{T}_{\text{back}}^{20\%} = \{t : t/T > 0.8\}. \quad (18)$$

The front-only control updates only the first 20% response tokens, while the back-only control updates only the last 20% response tokens. If attention entropy were merely acting as a positional proxy, these simple position-based masks should reproduce the main behaviors of entropy-defined anchor or explorer training.

Figure 7 shows the training dynamics of these position controls on Qwen3-8B-Base. Front-only training almost fails to learn: the reward remains close to the low-reward regime, response length quickly shrinks, and validation accuracy stays near zero across benchmarks. Back-only training is stronger than front-only training, indicating that answer-proximal tokens carry more direct outcome-relevant signal. However, it remains far below full-token DAPO and often degrades in later training, especially on harder benchmarks such as AIME and OLYMPIAD-BENCH.

These results rule out the interpretation that attention entropy is simply a proxy for response position. Position-only selection chooses a contiguous segment of the response and captures only where a token appears. In contrast, attention entropy selects tokens according to how they aggregate information from prior context. Low-entropy anchor tokens are therefore not merely early or late tokens; they provide stable concentrated-support updates across the response. Similarly, high-entropy explorer tokens are not equivalent to answer-proximal tokens; they reflect diffuse evidence aggregation and stronger but less stable optimization signals. Thus, the anchor/explorer distinction is not reducible to a trivial positional bias.

F.2 Prediction-Entropy Controls and Diagnostic Comparison

Another possible explanation is that attention entropy merely reflects output uncertainty. To separate attention-support entropy from prediction uncertainty, we define predictive entropy using the model’s next-token distribution before observing token y_t :

$$H_t^{\text{pred}} = - \sum_{v \in \mathcal{V}} p_{\theta}(v \mid x, y_{<t}) \log p_{\theta}(v \mid x, y_{<t}). \quad (19)$$

This quantity measures uncertainty over the next-token vocabulary distribution. In contrast, attention entropy is computed over the attention distribution across visible context positions and measures how concentrated or diffuse the token’s contextual support is:

$$H_t^{\text{attn}} = - \sum_{j=1}^{N_t} a_{t,j} \log a_{t,j}, \quad H_t^{\text{attn,norm}} = \frac{H_t^{\text{attn}}}{\log N_t}. \quad (20)$$

Thus, predictive entropy asks whether the model is uncertain about what token to generate next, whereas attention entropy asks whether the generated token is supported by a concentrated or diffuse set of prior context positions.

Prediction-entropy selective controls. We construct prediction-low and prediction-high controls by selecting the bottom and top 20% response tokens ranked by H_t^{pred} within each response:

$$\mathcal{T}_{\text{pred-low}}^{20\%} = \text{Bottom}_{20\%} \left(\{H_t^{\text{pred}}\}_{t=1}^T \right), \quad \mathcal{T}_{\text{pred-high}}^{20\%} = \text{Top}_{20\%} \left(\{H_t^{\text{pred}}\}_{t=1}^T \right). \quad (21)$$

We then repeat the same selective-training setup using these prediction-entropy-defined token groups in place of the attention-entropy-defined groups.

Figure 8 shows that grouping tokens by prediction entropy leads to a training profile that is different from the attention-entropy selective-training curves in Figure 2. Under the prediction-entropy

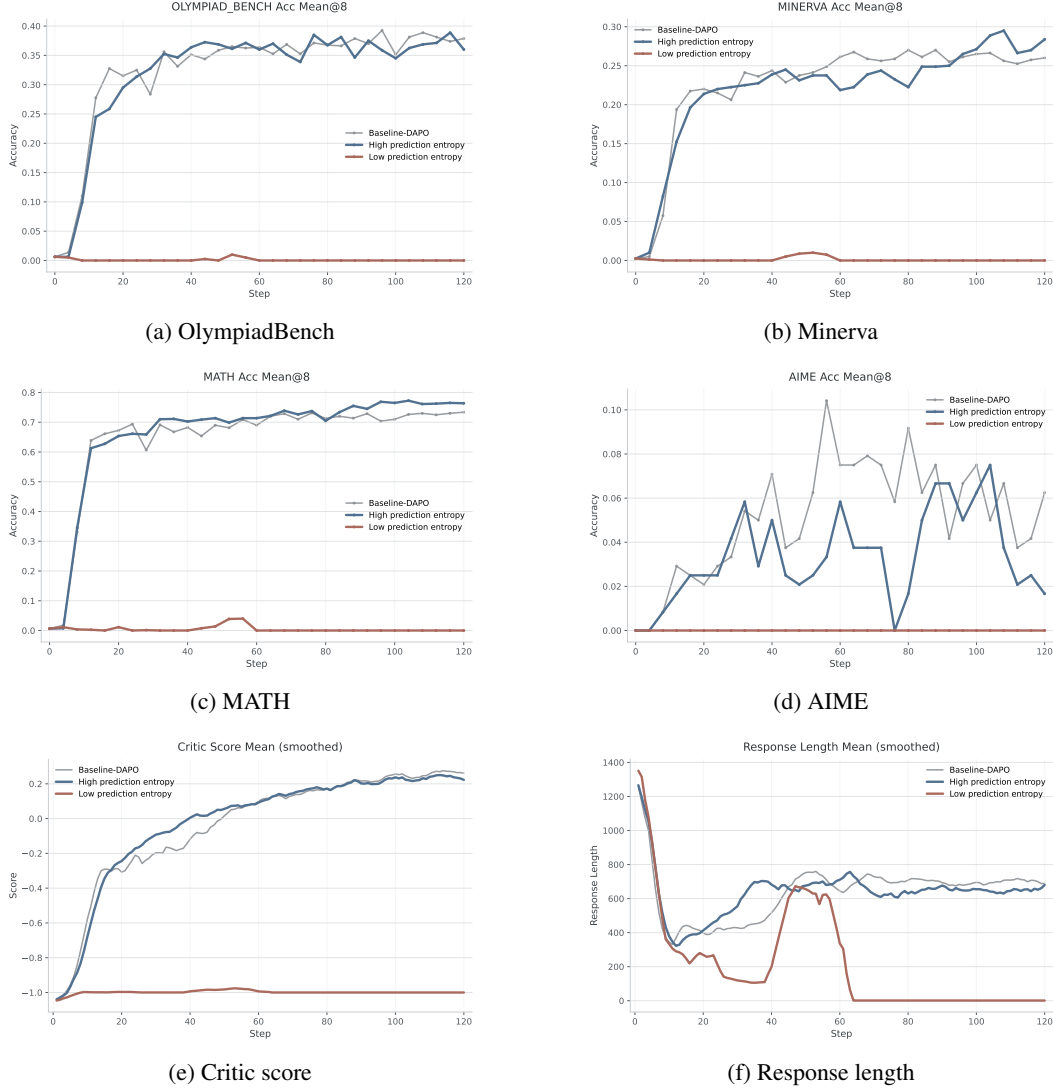


Figure 8: Prediction-entropy controls for selective token training. Tokens are selected by the entropy of the model’s next-token distribution rather than by attention entropy. The high-prediction-entropy and low-prediction-entropy subsets exhibit different training trajectories, separating output-distribution uncertainty from attention-support entropy.

partition, the high-prediction-entropy subset exhibits sustained changes in benchmark accuracy and critic score, while the low-prediction-entropy subset stays close to the floor on most metrics. Its response length also decreases sharply and eventually collapses to nearly zero. This pattern indicates that prediction-entropy selection mainly separates tokens according to uncertainty in the next-token output distribution.

This differs from the behavior induced by the attention-entropy partition. In the attention-entropy selective-training curves, low-attention-entropy and high-attention-entropy token groups show distinct optimization dynamics in terms of reward evolution, held-out accuracy, AIME behavior, response-length changes, and collapse patterns. The prediction-entropy controls do not reproduce this same form of separation. Instead, they reflect a different criterion: whether the model’s next-token distribution is sharp or uncertain at the current position.

Therefore, prediction entropy and attention entropy should be interpreted as two different token-level quantities. Prediction entropy characterizes uncertainty over the vocabulary distribution, whereas attention entropy characterizes the structure of contextual support across prior positions. The

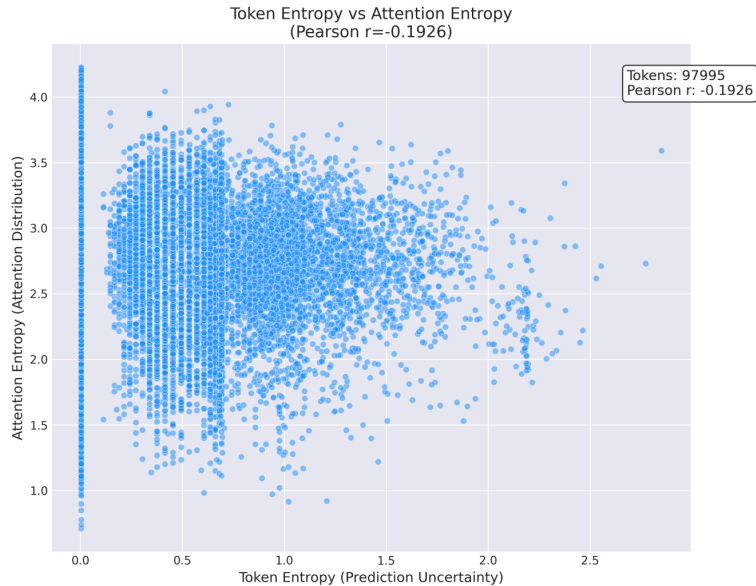


Figure 9: Token-level relation between predictive entropy and attention entropy. Each point corresponds to one response token. Across 97,995 tokens, the Pearson correlation is $r = -0.1926$, indicating a weak negative relationship rather than a strong alignment between the two scores. The broad dispersion of points shows that tokens with similar predictive entropy can have substantially different attention entropy, and vice versa. Thus, attention entropy is not simply a relabeling of next-token prediction uncertainty.

difference between the two sets of selective-training curves suggests that attention entropy is not fully explained by output uncertainty alone.

Global relation between attention entropy and prediction entropy. We first examine whether the two entropy scores define the same token ordering. Figure 9 plots token-level predictive entropy against attention entropy over response tokens. Across 97,995 tokens, the Pearson correlation is $r = -0.1926$, indicating only a weak negative linear relationship between the two quantities. This weak correlation suggests that predictive uncertainty and attention-support diffuseness are not interchangeable token-level signals.

The scatter structure shows that attention entropy and predictive entropy are related but non-equivalent token-level signals. Predictive entropy varies with the uncertainty of the output distribution, while attention entropy varies with the concentration or diffuseness of contextual support. Therefore, a token can be prediction-uncertain but attention-concentrated, or prediction-certain but attention-diffuse. The weak correlation in Figure 9 supports the view that attention-entropy-defined anchor/explorer groups cannot be reduced to low- or high-prediction-entropy tokens.

Quadrant analysis. To make the distinction more interpretable, we divide response tokens into four quadrants using within-response percentile thresholds for both entropy scores. Let HighPred and LowPred denote tokens above and below the median predictive entropy within the same response, and let HighAttn and LowAttn denote tokens above and below the median normalized attention entropy within the same response. This gives four token categories:

$$\begin{aligned}
 Q_{LP,LA} &= \text{LowPred} \cap \text{LowAttn}, \\
 Q_{HP,LA} &= \text{HighPred} \cap \text{LowAttn}, \\
 Q_{LP,HA} &= \text{LowPred} \cap \text{HighAttn}, \\
 Q_{HP,HA} &= \text{HighPred} \cap \text{HighAttn}.
 \end{aligned} \tag{22}$$



Figure 10: Quadrant analysis of predictive entropy and normalized attention entropy. Tokens are partitioned by within-response median thresholds. Word size indicates token frequency within each quadrant. The low-prediction / low-attention-entropy quadrant is dominated by routine reasoning-flow tokens; the high-prediction / low-attention-entropy quadrant contains discourse and planning tokens where the next-token choice is uncertain-despite concentrated support; the low-prediction / high-attention-entropy quadrant contains predictable but context-diffuse operation tokens; and the high-prediction / high-attention-entropy quadrant contains many symbolic or formula-heavy tokens with both output uncertainty and diffuse support. These qualitatively different token populations show that attention entropy does not simply relabel prediction entropy.

The resulting quadrants reveal qualitatively different token regimes rather than a simple monotonic relation between the two entropy scores. As shown in Figure 10, the low-prediction / low-attention-entropy quadrant is dominated by routine reasoning and problem-solving tokens, such as “need”, “number”, “equation”, “term”, “so”, and “because”. These tokens are relatively predictable from the output distribution and rely on concentrated contextual support, corresponding to a deterministic reasoning-flow regime.

The high-prediction / low-attention-entropy quadrant contains many discourse, planning, and transition tokens, such as “Maybe”, “Wait”, “But”, “Since”, “First”, “Then”, and “okay”. These tokens are uncertain at the output level, likely because multiple discourse continuations are plausible, yet their attention support remains concentrated. This quadrant therefore represents localized decision points: the model is uncertain about which token to emit, but the contextual evidence used by the token is not diffuse.

The low-prediction / high-attention-entropy quadrant shows the opposite off-diagonal pattern. It contains tokens such as “simple”, “possible”, “divide”, “minus”, “part”, and other operation-related or relation-related tokens. These tokens can be relatively easy to predict, while still aggregating information from a broader set of prior positions. This indicates that low predictive uncertainty does not imply concentrated attention support; some apparently certain tokens still depend on diffuse contextual aggregation.

Finally, the high-prediction / high-attention-entropy quadrant contains many formula-heavy, symbolic, or branching tokens, including fragments such as “frac”, “sqrt”, “left”, “right”, “theta”, “alpha”, “begin”, and “However”. This quadrant combines output uncertainty with diffuse contextual support, and corresponds to a more ambiguous regime where both the next-token choice and the contextual evidence distribution are less concentrated.

This quadrant view exposes cases that cannot be explained by output uncertainty alone. The two off-diagonal quadrants are especially important. High-prediction / low-attention-entropy tokens show that output uncertainty can arise even when a token relies on concentrated contextual support. Conversely, low-prediction / high-attention-entropy tokens show that a token can be easy to predict while still drawing on diffuse contextual evidence. Therefore, prediction entropy and attention entropy capture different axes of token behavior: the former measures uncertainty over the next-token distribution, whereas the latter measures the concentration of the contextual support used by the token representation.

Sequence-level dynamics. We also visualize both entropy scores along individual reasoning trajectories. Figure 11 shows one representative response, where the token background color indicates normalized attention entropy and the bottom bar indicates predictive entropy. This visualization reveals that the two signals follow different temporal patterns within the same reasoning trace.

At the beginning of the response, attention entropy is relatively high. This corresponds to an initial state-construction phase, where the model identifies the equation type, maps the coefficients, and establishes the problem-solving context. As the response enters routine algebraic computation, attention entropy tends to decrease, suggesting that these intermediate calculation tokens rely on more concentrated contextual support. Within calculation segments, we further observe a local rise–fall–rise pattern: attention entropy increases when a new calculation step is initiated, decreases during the middle of a stable local computation, and rises again when the computed result is integrated into the next reasoning step.

Predictive entropy exhibits a different behavior. Its peaks mark positions where the model is uncertain about the next-token choice, rather than positions where contextual support is necessarily diffuse. In the example, the erroneous token “e” in the fragment “ $x - 2 = e$ ” has high predictive entropy, suggesting that prediction entropy can act as a local warning signal for unstable or incorrect token generation. However, such prediction-entropy peaks do not generally coincide with attention-entropy peaks, indicating that output uncertainty and contextual-support diffuseness capture different aspects of token-level behavior.

The sequence-level visualization is intended as a qualitative diagnostic rather than a standalone statistical claim. Together with the global scatter and quadrant analyses, it suggests that prediction entropy and attention entropy can assign different roles to the same token positions: prediction entropy reflects local output uncertainty, whereas attention entropy reflects the diffuseness of contextual support.

Control conclusion. Overall, prediction entropy does not provide an equivalent substitute for attention entropy. Predictive entropy measures output-layer uncertainty, whereas attention entropy measures the internal concentration of contextual support. Their scatter distribution, quadrant composition, and sequence-level trajectories show only partial alignment. Moreover, prediction-entropy-based token selection does not reproduce the stable-anchor / fragile-explorer asymmetry induced by attention-entropy selection. This supports the interpretation that the anchor/explorer spectrum is not merely a confidence or uncertainty effect at the output layer, but is tied to how tokens aggregate evidence from prior context.

F.3 Loss-Magnitude Controls

Finally, we test whether the attention-entropy partition is simply a proxy for token-level objective magnitude. Let ℓ_t denote the per-token policy-gradient loss contribution. We rank tokens within each response by the magnitude of this contribution and construct two matched 20% token subsets:

$$\mathcal{T}_{\text{loss-low}}^{20\%} = \text{Bottom}_{20\%}(\{\ell_t\}_{t=1}^T), \quad \mathcal{T}_{\text{loss-high}}^{20\%} = \text{Top}_{20\%}(\{\ell_t\}_{t=1}^T). \quad (23)$$

We then repeat the same selective-training setup using these loss-magnitude groups in place of the attention-entropy groups.

Dual Entropy: Thinking process: Solve the eq...

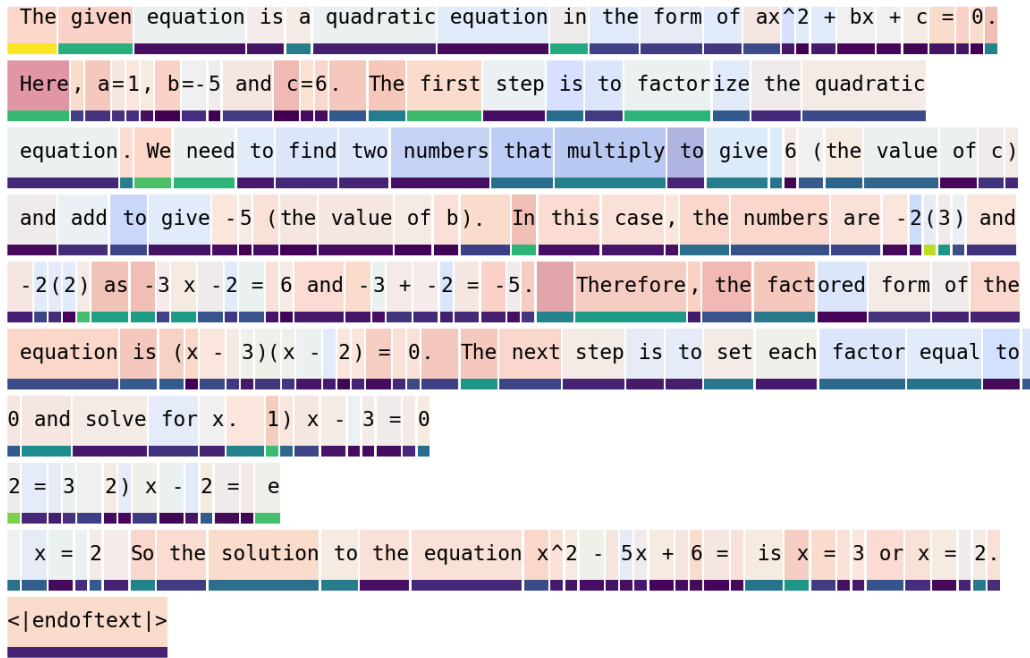


Figure 11: Sequence-level visualization of normalized attention entropy and predictive entropy along a reasoning trace. Background color denotes attention entropy, while the bottom bar denotes predictive entropy. Attention entropy is higher during initial state construction and reasoning-stage transitions, decreases during stable local computation, and can rise again when an intermediate result is integrated into the next step. Predictive entropy instead highlights local uncertainty over the next-token choice; for example, the erroneous token “e” in “ $x - 2 = e$ ” appears with high predictive entropy. The two signals therefore capture different aspects of token-level behavior.

Figure 12 shows the behavior of selective training when tokens are grouped by instantaneous loss magnitude rather than by attention entropy. The high-loss-only variant exhibits gradual improvement on OlympiadBench, Minerva, MATH, AIME, and critic score, indicating that tokens with large policy-gradient loss contributions contain direct update signal. In contrast, the low-loss-only variant stays close to zero accuracy across all benchmarks, while its critic score remains near the floor. This pattern is consistent with the intended role of this control: loss-magnitude selection primarily separates tokens by the strength of their immediate optimization contribution.

This behavior is qualitatively different from the attention-entropy-based selective-training curves in Figure 2. The entropy-based split does not simply reproduce a high-loss versus low-loss separation. Instead, it yields a different set of training dynamics: low-entropy and high-entropy token groups differ in stability, collapse behavior, response length evolution, and benchmark-specific trajectories. By contrast, the loss-magnitude split mainly distinguishes whether the selected tokens carry large or small instantaneous policy-gradient contributions.

Therefore, these controls suggest that attention entropy is not merely acting as a surrogate for per-token loss magnitude. Loss magnitude characterizes the immediate strength of the token-level



Figure 12: Loss-magnitude controls for selective token training. Tokens are selected by the magnitude of their per-token policy-gradient loss contribution rather than by attention entropy. High-loss-only training shows gradual improvement, whereas low-loss-only training remains close to the floor across benchmarks and critic score.

objective signal, whereas attention entropy characterizes the structure of attention support used by a token when aggregating contextual evidence. The difference between the two sets of curves indicates that the entropy partition captures a token property that is distinct from instantaneous loss scale.

G Normalization Controls and Full Optimization Trajectories

G.1 Normalization variants

A potential confound in masked token-level training is the normalization denominator. Let $m_t \in \{0, 1\}$ denote the subset mask, T the number of response tokens, and $K = \sum_{t=1}^T m_t$ the number of selected tokens. For a per-token loss contribution ℓ_t , we compare two normalization schemes:

$$\mathcal{L}_{\text{subset}}^{\text{sel}} = \frac{1}{K} \sum_{t=1}^T m_t \ell_t, \quad (24)$$

and

$$\mathcal{L}_{\text{subset}}^{\text{all}} = \frac{1}{T} \sum_{t=1}^T m_t \ell_t. \quad (25)$$

The selected-token mean in Eq. 24 preserves the average loss scale over the retained tokens. In contrast, the all-token mean in Eq. 25 keeps the denominator equal to the full response length and therefore shrinks the total subset contribution. Since our masks retain 20% of response tokens, $K \approx 0.2T$, and selected-token normalization increases the effective update scale of the retained tokens by approximately $5\times$ relative to all-token normalization.

These two variants answer complementary questions. The all-token mean tests whether a subset remains effective even when its contribution is diluted by the full response length. The selected-token mean tests the intrinsic training quality of the retained tokens after removing this dilution effect, but it also introduces a larger effective update scale. Comparing both variants allows us to separate genuine subset quality from a normalization-induced scale artifact.

G.2 Full optimization trajectories

Figure 13 compares full-token DAPO with low-attention-entropy and high-attention-entropy 20% token subsets under both normalization variants. Runs with the suffix `AllTokenMean` use Eq. 25; runs without this suffix use Eq. 24.

The main observation is that the low-vs-high attention-entropy gap persists under both normalization schemes. Low-attention-entropy training remains strong and stable under both selected-token and all-token normalization. It achieves held-out performance close to full-token DAPO on the averaged validation score, maintains relatively stable response lengths, and does not exhibit large gradient spikes. This indicates that low-entropy anchor tokens provide robust optimization signals rather than benefiting from a particular normalization choice.

High-attention-entropy training behaves differently. Under all-token normalization, high-attn training is weak: the subset contribution is diluted, the reward remains low, response lengths often collapse to short traces, and held-out accuracy stays far below both low-attn training and full-token DAPO. However, under selected-token normalization, simply restoring the per-token scale does not make high-attn training stable. Instead, high-attn training exhibits much larger gradient norms, abrupt response-length spikes, and unstable reward dynamics. Thus, high-attn tokens do not fail merely because their gradients are too small under all-token normalization. When their update scale is restored, their signals become stronger but not more reliable.

This comparison supports the interpretation that low-entropy anchors and high-entropy explorers play different optimization roles. Low-entropy anchors provide concentrated-support updates that are stable across normalization choices. High-entropy explorers carry stronger and more volatile signals that are difficult to use in isolation. Therefore, the anchor/explorer distinction is not an artifact of the loss normalization denominator.

G.3 Characteristic failure modes of explorer-only training

The normalization comparison also clarifies the failure modes of explorer-only training. High-attention-entropy tokens are not simply uninformative. Under selected-token normalization, their gradient norms can become much larger than those of full-token DAPO or low-attn training, indicating that these tokens indeed carry strong optimization pressure. However, this pressure is difficult to use in isolation and often manifests as unstable training dynamics.

We observe three recurring failure modes. First, some runs enter an early short-response collapse, where response length rapidly shrinks and reward growth stalls. Second, some runs show abrupt length instability, with sudden spikes in generated length followed by reward degradation. Third, some runs undergo gradual reasoning degeneration, where validation accuracy initially improves but later declines as the policy drifts toward less reliable reasoning patterns. These behaviors are consistent with the view that high-entropy explorer tokens aggregate diffuse evidence and produce high-variance updates.

Rare successful explorer-only runs avoid these failure modes. They maintain longer reasoning traces, recover reward growth, and can sometimes achieve strong performance on difficult benchmarks such as AIME. We interpret this as evidence of potential signal rather than method competitiveness: explorer tokens are not simply uninformative, but their useful contribution is difficult to extract when they are isolated from lower-entropy stabilizing updates. This motivates using a stable optimization backbone or a softer weighting strategy rather than relying on isolated hard masking.

G.4 Interpretation

Overall, normalization modulates the severity of subset training but does not create or remove the entropy-defined optimization spectrum. All-token normalization is conservative and can dilute sparse updates, while selected-token normalization restores the per-token loss scale but can amplify unstable signals. Low-attn anchors remain robust under both choices, whereas high-attn explorers are either too weak under all-token normalization or too volatile under selected-token normalization.

This supports the central interpretation of our analysis: attention entropy does not merely select tokens with a favorable normalization scale. Instead, it separates response tokens along a structural optimization axis. Low-entropy tokens provide stable concentrated-support updates that can serve

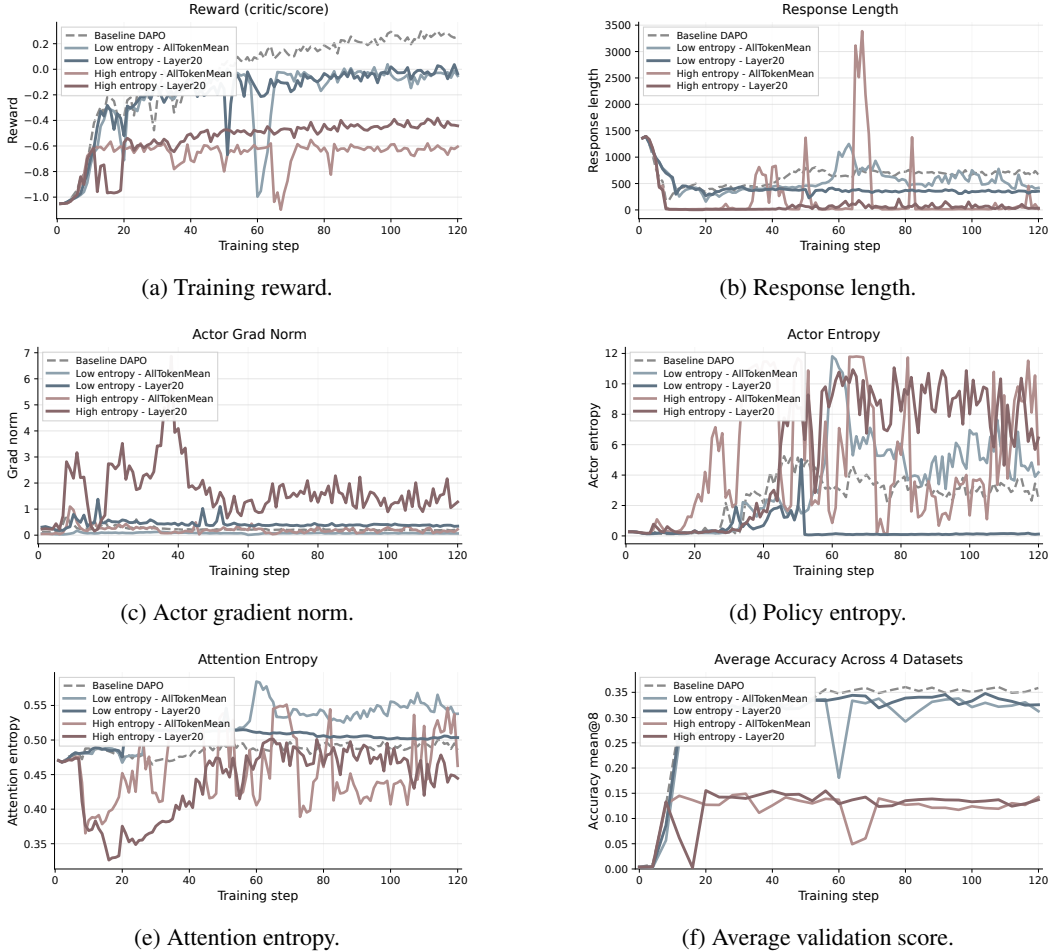


Figure 13: Normalization controls for low-attention-entropy and high-attention-entropy 20% token subsets on Qwen3-8B-Base. Curves with the suffix AllTokenMean use all-token normalization $\mathcal{L}_{\text{subset}}^{\text{all}}$, while curves without this suffix use selected-token normalization $\mathcal{L}_{\text{subset}}^{\text{sel}}$. Low-attn training remains stable and competitive under both normalization schemes. High-attn training is weak under all-token normalization and becomes much more volatile under selected-token normalization, with large gradient spikes and erratic response-length behavior. These results indicate that the anchor/explorer distinction is not caused by the normalization denominator.

as an optimization backbone. High-entropy tokens provide broader, stronger, but higher-variance signals that are difficult to exploit through hard masking alone. This motivates the entropy-aware soft-reweighting validation intervention, where stable anchor-like updates are emphasized early while broader explorer-like signals are gradually incorporated later in training.

H Additional Evidence-Gathering Analyses

H.1 Robustness across entropy definitions

In the main paper, we use normalized attention entropy as the default score for defining anchor and explorer tokens. A potential concern is that different entropy definitions may capture different aspects of attention behavior. In particular, normalized entropy divides raw entropy by $\log N_t$, where N_t is the number of visible positions, and therefore measures concentration relative to the available context length. Raw entropy, in contrast, has an upper bound that grows with N_t and can therefore be affected by token position and visible-context length. To examine whether our evidence-gathering conclusions are specific to one entropy definition, we repeat the analysis under four variants: normalized attention

Table 11: Explorer-only multi-seed statistics over $N = 8$ independent runs. A run is considered successful if it avoids collapse according to the criterion defined in this appendix. Because most explorer-only runs collapse, the successful-run statistics are reported only as a conditional diagnostic of potential signal quality, not as an overall method comparison. Avg. w/o AIME denotes the arithmetic mean over OlympiadBench, Minerva, and MATH.

Metric	Value
Total runs	8
Successful runs	3
Success rate	37.5%
<i>Successful runs</i>	
AIME (mean \pm std)	12.31 ± 0.53
Avg. w/o AIME (mean \pm std)	46.13 ± 1.58
AIME – full-token	6.48
<i>Failed runs</i>	
First detected collapse step	21.80 ± 3.84

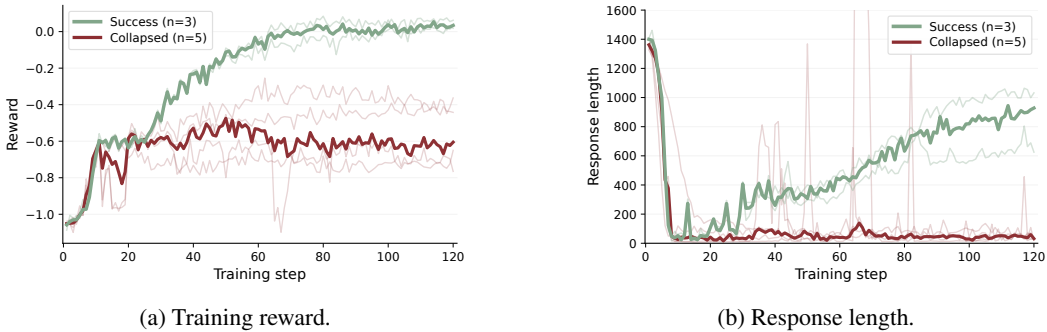


Figure 14: Explorer-only training exhibits a bimodal optimization pattern across $N = 8$ independent seeds. Successful runs (green, $n = 3$) recover normal reward growth and maintain long reasoning traces, while collapsed runs (red, $n = 5$) fail to sustain learning and rapidly degenerate into very short responses. Thick curves denote group averages, and faint curves denote individual runs.

entropy, raw attention entropy, raw attention entropy restricted to the first 512 response tokens, and top-256 raw attention entropy.

Across all variants, the support-concentration pattern is consistent: anchor tokens require fewer support positions to accumulate the same amount of attention mass, whereas explorer tokens require more support positions. This confirms that the anchor–explorer distinction is robustly tied to effective support size. In contrast, spatial-span statistics are less stable across entropy definitions. Under normalized entropy, anchors can appear slightly more non-local, reflecting sparse support relative to a long visible context. Under raw entropy, explorers appear more non-local, partly because raw entropy is affected by the growth of the visible context. Restricting the analysis to the first 512 response tokens reduces this position-length effect, while top-256 raw entropy further focuses on the dominant attention support and weakens the distance-based separation. These results support the interpretation in Section 4: attention entropy should primarily be viewed as a measure of support concentration rather than attention distance.

Normalized attention entropy. Figure 15 shows the evidence-gathering pattern under the default normalized attention entropy used in the main paper. Anchor tokens require substantially fewer support positions than explorer tokens at all attention-mass thresholds, confirming the sparse-versus-diffuse support distinction. Spatially, anchors are not more local under this definition; they show slightly larger average attention distance, lower local mass, and higher non-local mass. This indicates that normalized entropy captures relative support concentration rather than locality.

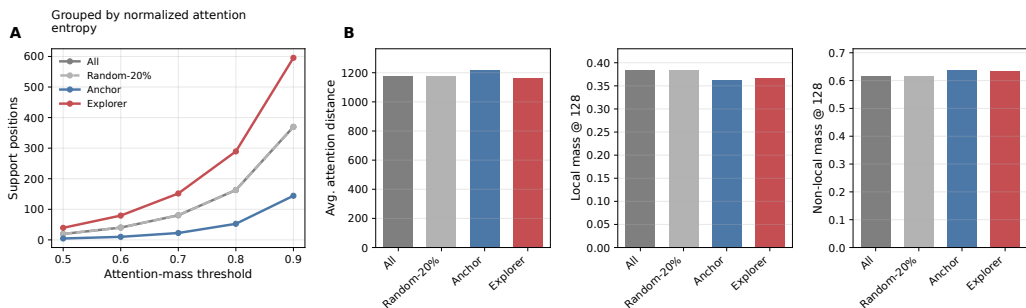


Figure 15: Evidence-gathering patterns grouped by normalized attention entropy. (A) Anchor tokens require far fewer support-gathering positions than explorer tokens to accumulate the same attention mass, indicating concentrated support. Explorer tokens require many more support positions, indicating diffuse aggregation. (B) Under normalized entropy, anchors are not more local: they have slightly larger average attention distance, lower local-window mass, and higher non-local mass. This suggests that normalized entropy captures relative support concentration rather than attention locality.

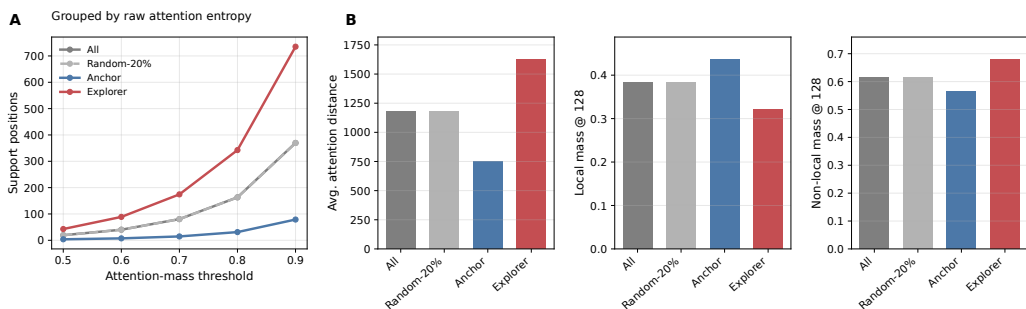


Figure 16: Evidence-gathering patterns grouped by raw attention entropy. (A) The sparse-versus-diffuse support distinction remains clear: anchors require fewer support positions, while explorers require more. (B) In contrast to normalized entropy, raw entropy makes explorers appear more non-local, with larger average attention distance and higher non-local mass. Since the upper bound of raw entropy increases with the number of visible positions, this spatial pattern may partly reflect position and visible-context-length effects.

Raw attention entropy. Figure 16 repeats the analysis using raw attention entropy. The concentration pattern remains unchanged: anchors require fewer support positions and explorers require more. However, the spatial-span pattern differs from normalized entropy. Under raw entropy, explorer tokens show much larger average attention distance and higher non-local mass, while anchors appear more local. This difference should be interpreted cautiously because the upper bound of raw entropy grows with the number of visible positions. Therefore, raw entropy can partially reflect token position and visible-context length.

Raw attention entropy in the first 512 response tokens. To reduce the visible-context-length confound in raw entropy, we repeat the raw-entropy analysis using only the first 512 response tokens. Figure 17 shows that the concentration pattern again remains stable: anchors require fewer support positions, while explorers require more. The spatial-span gap becomes much smaller than in the full raw-entropy analysis. Explorers still show somewhat larger average attention distance and higher non-local mass than anchors, but the difference is substantially reduced. This suggests that part of the strong non-local pattern under raw entropy comes from position and context-length effects.

Top-256 raw attention entropy. Finally, we compute entropy using only the top-256 attention weights, after renormalizing them. This focuses the entropy measure on the dominant support positions and reduces the influence of long-tail attention mass. Figure 18 again shows the same concentration pattern: anchors require fewer support positions and explorers require more. However, distance-based differences are relatively weak. This further supports the conclusion that entropy-

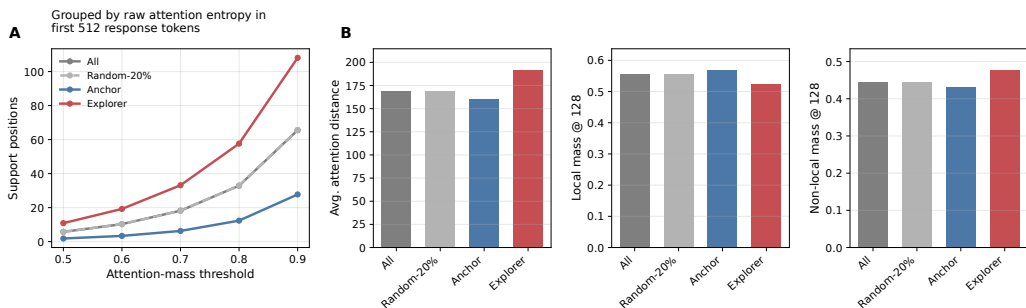


Figure 17: Evidence-gathering patterns grouped by raw attention entropy within the first 512 response tokens. (A) Anchor tokens still require fewer support positions than explorer tokens, showing that the concentration-based distinction persists when restricting the analysis to early response tokens. (B) The distance-based separation is weaker than in the full raw-entropy analysis, suggesting that visible-context-length and position effects contribute to the strong spatial-span pattern observed under raw entropy.

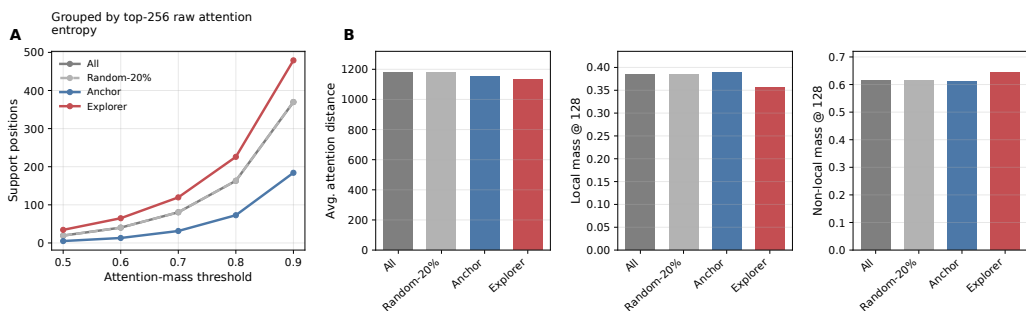


Figure 18: Evidence-gathering patterns grouped by top-256 raw attention entropy. (A) The support-concentration distinction remains robust: anchors require fewer support positions and explorers require more. (B) Spatial-span differences are weaker under top-256 entropy, indicating that the main stable distinction between anchors and explorers is effective support size rather than attention distance.

defined token groups are robustly separated by effective support size, while spatial locality is not the primary or stable axis of separation.

Summary. Taken together, these variants show that the anchor–explorer distinction is robust along the support-concentration axis but not along a fixed locality axis. Across normalized entropy, raw entropy, first-512 raw entropy, and top-256 raw entropy, anchors consistently use fewer effective support positions, whereas explorers aggregate over more positions. However, whether anchors or explorers appear more non-local depends on the entropy definition. We therefore avoid interpreting attention entropy as a direct measure of attention distance. Instead, we interpret it as a diagnostic for effective support concentration, which is the property most consistently associated with the observed optimization spectrum.

H.2 Spatial-span diagnostics are secondary to support concentration

The figures above also provide additional spatial-span diagnostics, including average attention distance, local-window mass, and non-local mass. These statistics are useful for checking whether attention entropy can be reduced to a simple local-versus-global distinction. The answer is negative: spatial-span patterns vary substantially across entropy definitions.

Under normalized attention entropy (Figure 15), anchor tokens have slightly larger average attention distance, lower local mass, and higher non-local mass than explorer tokens. This means that low normalized entropy does not imply local attention. A token can have low normalized entropy by

placing highly concentrated attention on a small number of salient positions, even if those positions are distant in the context.

Under raw attention entropy (Figure 16), the ordering reverses: explorer tokens appear much more non-local. This is expected because raw entropy grows with the number of visible positions and is therefore more sensitive to response position and context length. When we restrict the raw analysis to the first 512 response tokens (Figure 17), this distance-based gap becomes much smaller, indicating that part of the raw-entropy spatial pattern comes from visible-context-length effects rather than from an intrinsic locality property of the token group. When entropy is computed only over the top-256 attention weights (Figure 18), distance-based differences are further weakened.

These results reinforce the main interpretation in Section 4. Attention entropy should not be treated as a direct locality score. Its most stable diagnostic role is to distinguish tokens with sparse selective support from tokens with diffuse multi-position aggregation. Spatial-span statistics help rule out an overly simple local-versus-global interpretation, but they are not the defining axis of the anchor-explorer distinction.

H.3 Qualitative attention-map case studies

We further provide qualitative attention-map examples to illustrate the evidence-gathering modes captured by attention entropy. These examples are not intended as standalone causal evidence; rather, they visually complement the quantitative support-concentration analyses in Appendix H.1 and Appendix H.2.

Figure 19 shows two selected tokens from the same reasoning trajectory: one anchor token from the bottom 20% of within-response normalized attention entropy, and one explorer token from the top 20%. For each selected token, we visualize its attention distribution over previous tokens. The cells are ordered by their original positions in the trajectory, and the color intensity indicates the attention mass assigned by the current token to each history token.

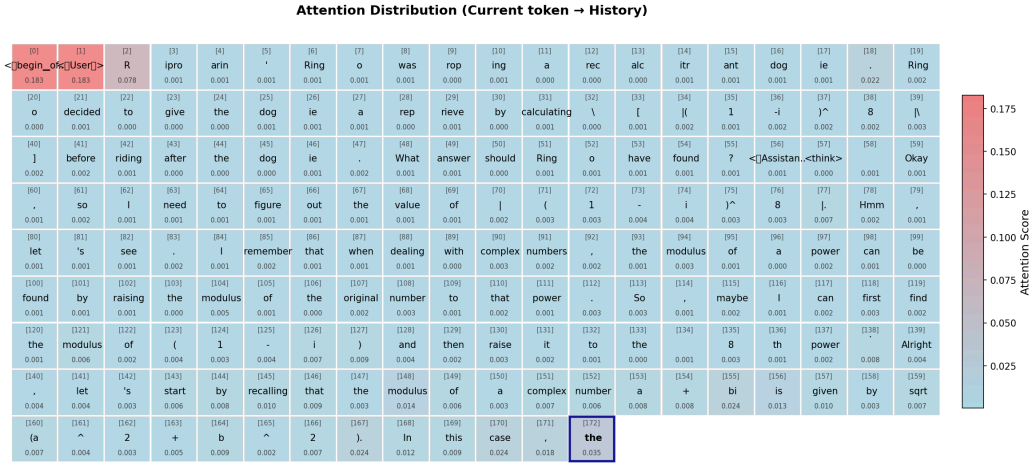
The anchor example illustrates sparse selective support. Its attention mass is concentrated on a small number of salient positions in the reasoning chain, which may include nearby tokens or distant earlier states. In contrast, the explorer example illustrates diffuse multi-position aggregation: its attention is spread over multiple non-adjacent positions, such as problem quantities, operators, intermediate results, and previously derived expressions. This qualitative pattern is consistent with the quantitative observation that anchor tokens require fewer support positions to accumulate a fixed amount of attention mass, whereas explorer tokens require more.

Interpretation: evidence-gathering modes and reasoning operations. The evidence-gathering analyses above suggest an operational interpretation of the anchor-explorer distinction. Anchor tokens correspond to reasoning operations that can be supported by a small number of salient positions, such as continuing along an established derivation, consolidating an intermediate quantity, or confirming a previously derived result. These support positions may be nearby or distant, depending on the entropy definition and the specific trajectory, but the effective support remains selective. Such operations are frequent and tend to produce reusable, low-variance optimization signals.

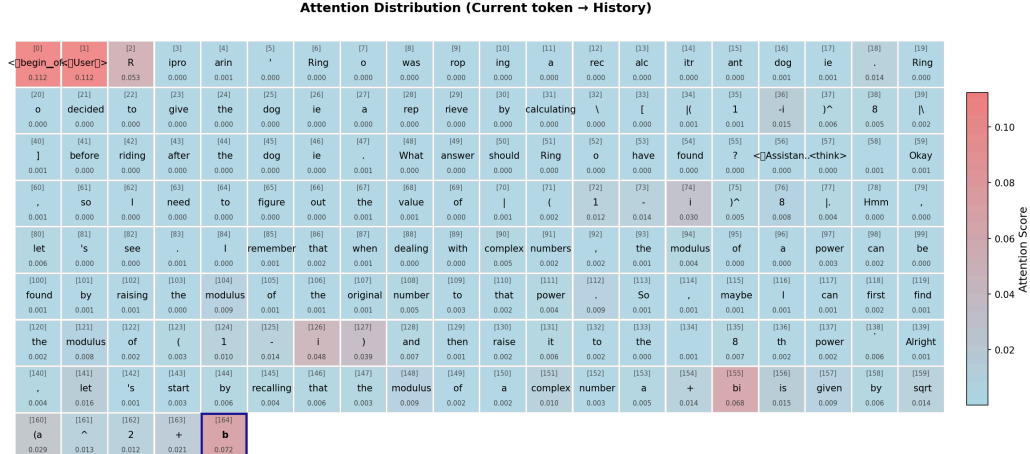
Explorer tokens, in contrast, correspond to operations that require diffuse multi-position aggregation, such as combining several intermediate results, checking consistency across distant reasoning steps, or integrating multiple partial states before making a new inference. These operations are less frequent and more trajectory-dependent. This interpretation helps explain the optimization asymmetry observed in the main experiments: anchor-only training is stable because it preserves a reliable selective-support backbone, whereas explorer-only training is fragile because it isolates broader but more context-sensitive signals. At the same time, the complementary information carried by explorer tokens can be useful in successful runs, especially on harder reasoning benchmarks.

I Additional Entropy Dynamics

In the main paper, we report entropy dynamics using normalized attention entropy, which is the default metric used to define anchor and explorer tokens. Here we provide additional entropy-dynamics analyses under alternative entropy definitions: raw attention entropy, top- k attention entropy, and fixed-position entropy. These variants serve two purposes. First, they test whether the mean separation



(a) **Anchor token.** Low-entropy token from the same reasoning trajectory. The attention mass is concentrated on a small set of salient support positions.



(b) **Explorer token.** High-entropy token from the same reasoning trajectory. The attention mass is distributed across many non-adjacent support positions.

Figure 19: Qualitative attention-map case study from a single reasoning trajectory. We compare one anchor token and one explorer token selected by within-response normalized attention entropy. Each panel visualizes the attention distribution from the selected current token to its history tokens. The anchor token exhibits sparse selective support, concentrating attention on a small number of salient positions. The explorer token exhibits diffuse multi-position aggregation, spreading attention across multiple separated reasoning states. These examples illustrate that the anchor–explorer distinction is better understood as sparse versus diffuse support, rather than as a simple local-versus-global attention pattern.

between anchor, full, and explorer tokens is specific to normalized entropy. Second, they help separate support-concentration effects from normalization and visible-context-length effects.

Across these variants, the most robust observation is the persistence of mean entropy separation: explorer tokens remain the highest-entropy group, anchor tokens remain the lowest-entropy group, and full tokens lie in between. This confirms that RL training does not collapse all response tokens into a uniform attention regime. Instead, the separation between sparse-support and diffuse-support token groups is preserved throughout training.

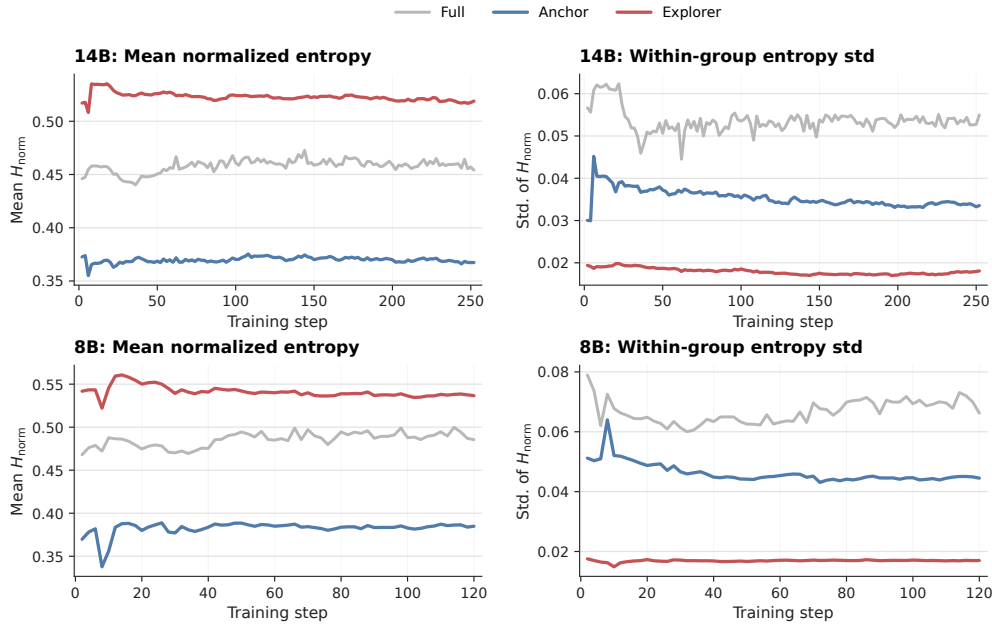


Figure 20: Dynamics of normalized attention entropy during RL training. We report the mean normalized entropy and the within-group entropy standard deviation for full response tokens, anchor tokens, and explorer tokens on Qwen3-14B and Qwen3-8B. Across both model scales, the mean entropy remains clearly separated throughout training: explorer tokens maintain the highest normalized entropy, anchor tokens maintain the lowest, and full tokens lie in between. The standard deviation measures dispersion of scalar entropy values within each group, not optimization volatility.

At the same time, the within-group standard deviation should be interpreted carefully. It measures dispersion of scalar entropy values within a group, not optimization volatility. In several settings, explorer tokens form a relatively narrow high-entropy band and therefore have smaller entropy-value variance than full or anchor tokens. This does not imply that explorer-only training is optimization-stable. Rather, explorer instability is captured by selective-training outcomes and gradient-level alignment dynamics, not by the scalar entropy variance itself.

I.1 Raw entropy dynamics

Raw attention entropy provides the most direct measure of absolute attention spread, but it is also the most sensitive to sequence length. Since the number of visible positions grows during generation, the upper bound of raw entropy also increases with token position. Therefore, raw entropy mixes two effects: genuine attention dispersion and visible-context-length growth.

Despite this confound, Figure 21 shows that the anchor–explorer ordering remains broadly consistent. Explorer tokens maintain higher raw entropy than anchor tokens, while full tokens lie between them or approach explorer entropy in later training. This indicates that the high-entropy group continues to represent a more diffuse support regime under the unnormalized metric.

The standard-deviation curves further illustrate why raw entropy is not ideal as the main metric. Full tokens show large variance because they contain the entire entropy spectrum and because raw entropy is strongly affected by token position. In contrast, anchor and explorer subsets are narrower by construction. Thus, raw-entropy variance should not be interpreted as optimization stability or instability. Instead, raw entropy is useful mainly as a robustness check showing that the mean separation is not unique to normalized entropy.

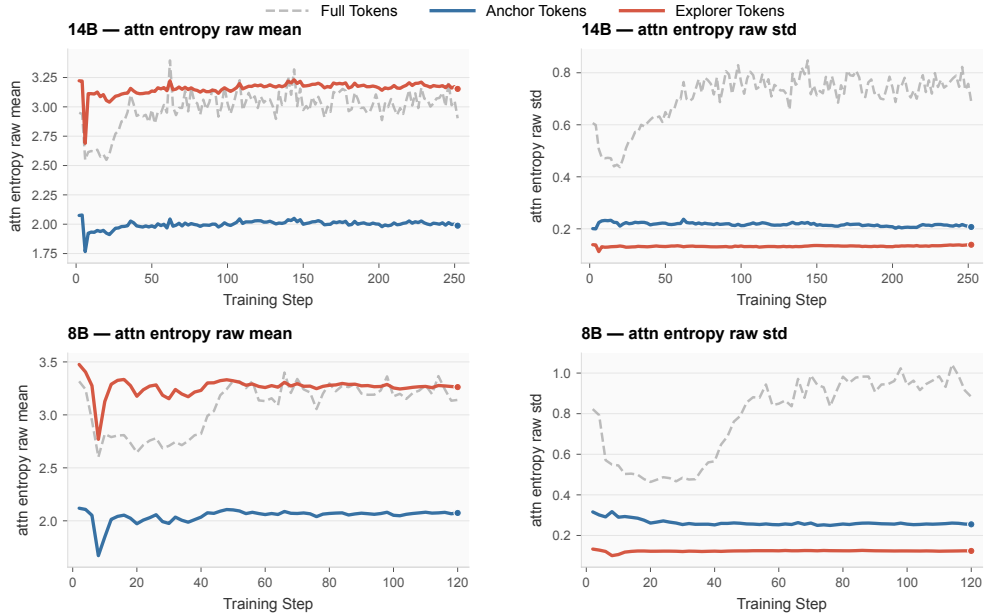


Figure 21: Raw attention entropy dynamics. We report the mean raw entropy and within-group raw-entropy standard deviation for full tokens, anchor tokens, and explorer tokens on Qwen3-14B and Qwen3-8B. The mean separation between explorer, full, and anchor tokens remains visible: explorer tokens generally maintain the highest raw entropy, while anchor tokens maintain the lowest. However, raw entropy is sensitive to visible-context length because its theoretical upper bound grows with the number of visible positions. As a result, the full-token population exhibits substantially larger variance and stronger non-stationarity under raw entropy. This supports using raw entropy as a diagnostic variant rather than as the primary grouping metric.

I.2 Top- k entropy dynamics

Top- k entropy focuses on the dominant attention support by discarding the long tail of very small attention weights. This makes it a useful complement to raw and normalized entropy: if the anchor-explorer separation remains visible under top- k entropy, then the distinction is not driven only by low-mass attention tails.

Figure 22 shows that this separation is indeed preserved. Explorer tokens consistently have higher top- k entropy, indicating that even among the dominant attended positions, they aggregate over a broader support set. Anchor tokens remain low-entropy, indicating concentrated dominant support. Full tokens remain between the two groups.

The standard-deviation curves show that explorer tokens can occupy a relatively narrow high-entropy band under top- k entropy. This is consistent with the main normalized-entropy dynamics: explorer tokens are not necessarily diverse in scalar entropy value, but they remain distinct in support regime. Their optimization fragility should therefore be attributed to the gradient effects of diffuse support aggregation rather than to larger entropy-value variance.

I.3 Fixed-position entropy dynamics

Fixed-position entropy controls for the fact that later tokens can attend to more previous positions. By restricting the computation to a fixed number of visible positions, this variant reduces the visible-context-length confound that affects raw entropy and can also influence normalized entropy.

Figure 23 shows that the mean separation persists under this control. Explorer tokens retain the highest fixed-position entropy, anchor tokens retain the lowest, and full tokens remain in between. This indicates that the anchor-explorer distinction is not simply caused by different numbers of

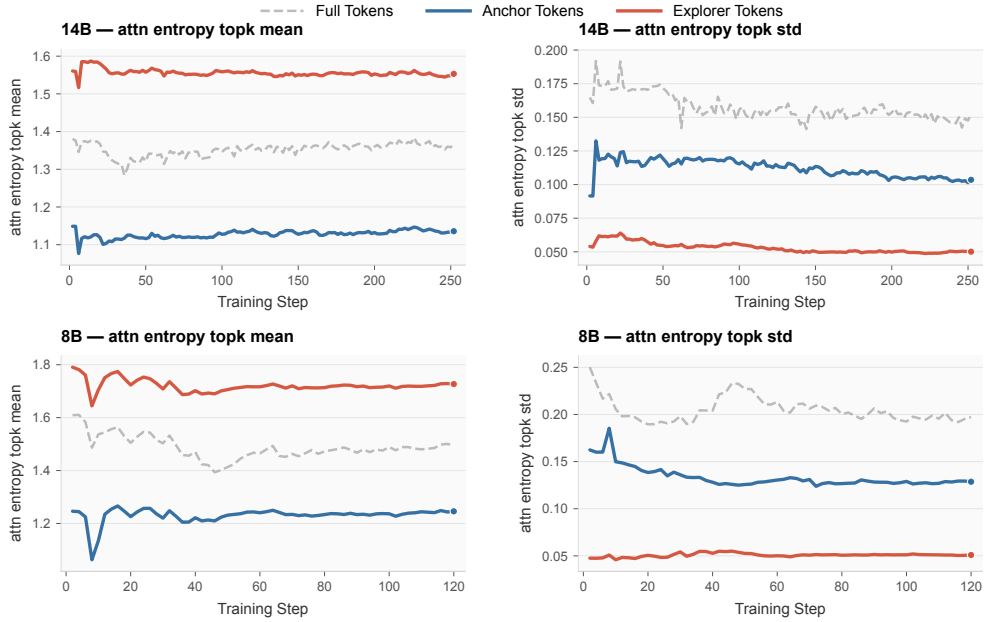


Figure 22: Top- k attention entropy dynamics. We compute entropy using the top- k attention weights after renormalization, focusing on the dominant attention support. Across both Qwen3-14B and Qwen3-8B, explorer tokens maintain the highest top- k entropy, anchor tokens maintain the lowest, and full tokens remain in between. This indicates that the anchor-explorer separation is preserved even when measuring only the dominant support structure rather than the full attention distribution. The within-group standard deviation again reflects scalar entropy dispersion, not optimization volatility.

visible positions. Instead, it reflects a genuine difference in how concentrated or diffuse the effective attention support is.

The standard-deviation curves again reinforce the same caution: scalar entropy variance is not the same as optimization volatility. Full tokens can have high variance because they cover the whole spectrum. Anchor and explorer subsets can each be relatively narrow in entropy value while still producing very different optimization behavior. The role of fixed-position entropy is therefore not to explain explorer fragility directly, but to verify that the support-regime separation remains after reducing length-related confounds.

I.4 Summary

Taken together, the alternative entropy definitions support three conclusions.

First, the mean separation between anchor, full, and explorer tokens is robust. Across raw entropy, top- k entropy, and fixed-position entropy, explorer tokens consistently occupy a higher-entropy regime, anchor tokens occupy a lower-entropy regime, and full tokens lie between them. This supports the claim that RL training preserves an entropy-defined support spectrum rather than collapsing all tokens into a single attention regime.

Second, entropy-value standard deviation should not be used as a direct proxy for optimization instability. Explorer tokens often form a narrow high-entropy band, meaning that their scalar entropy values can be relatively homogeneous. Their training fragility instead comes from optimization-level behavior: diffuse multi-position support can produce trajectory-sensitive gradients, low alignment with the full-token update direction, and collapse-prone selective-training dynamics.

Third, different entropy definitions emphasize different confounds. Raw entropy is sensitive to visible-context length; top- k entropy focuses on dominant support and reduces the influence of long-tail attention mass; fixed-position entropy controls for context-length growth. The fact that the

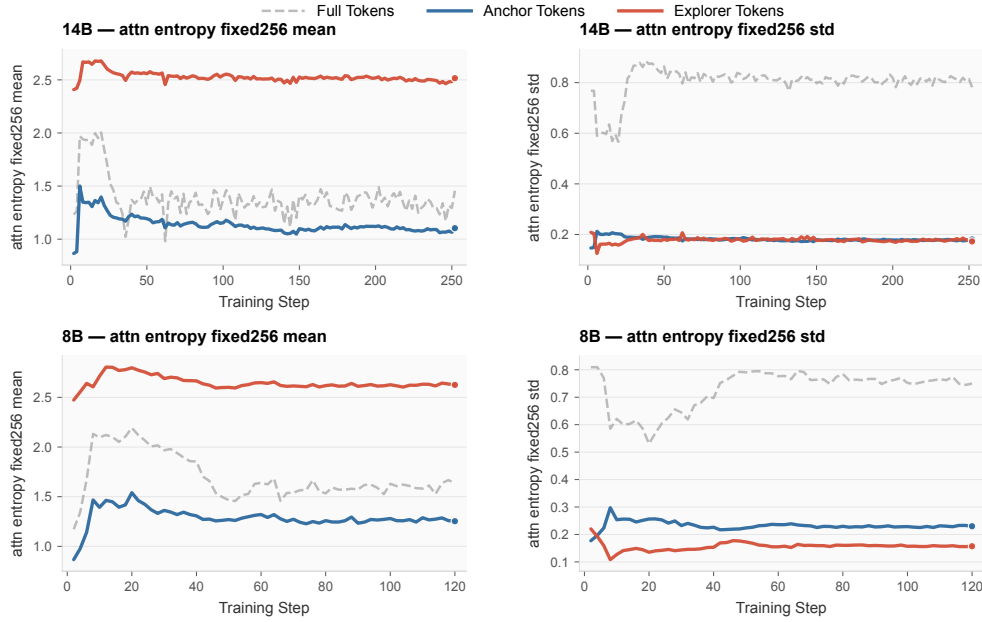


Figure 23: Fixed-position entropy dynamics. We compute entropy after restricting attention to a fixed set of visible positions, reducing the influence of visible-context-length growth. The mean entropy separation remains clear: explorer tokens retain higher fixed-position entropy, anchor tokens retain lower fixed-position entropy, and full tokens lie in between. This provides evidence that the anchor-explorer separation is not merely an artifact of increasing context length during generation.

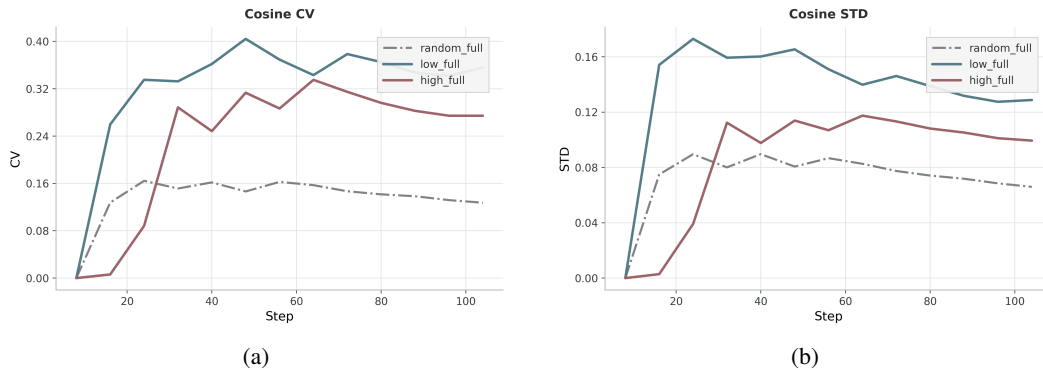


Figure 24: Online directional statistics of gradient-probe trajectories. We summarize the temporal variation of cosine similarity between each subset gradient and the full-token gradient using coefficient of variation (CV) and standard deviation (STD). Random-20% subsets show the lowest variation, consistent with stable sparse approximation of the full-token update. Entropy-defined subsets show larger directional non-stationarity: anchor gradients exhibit the strongest temporal drift, while explorer gradients remain less stable than random subsets and pass through the low-alignment regime shown in Figure 4.

mean separation persists across these variants strengthens the interpretation that attention entropy captures a robust support-concentration axis.

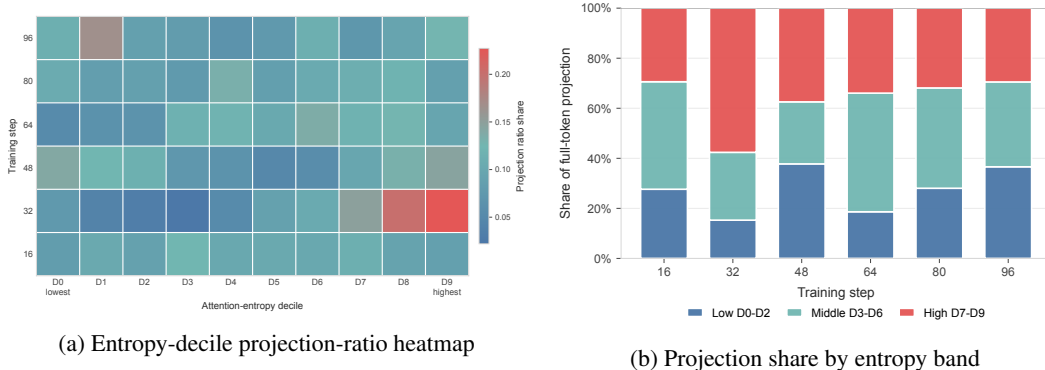


Figure 25: **Decile-level gradient decomposition along the attention-entropy axis.** (a): projection-ratio heatmap over entropy deciles and training steps. Each cell shows how much the gradient induced by one entropy decile contributes along the full-token gradient direction. (b): the same projection-ratio statistics aggregated into low-entropy (D0–D2), middle-entropy (D3–D6), and high-entropy (D7–D9) bands and normalized into shares. The results reveal a structured but stage-dependent entropy spectrum: upper-entropy deciles often contribute strongly, especially in early-to-middle training, but useful gradient contribution remains distributed across the spectrum rather than concentrated in a fixed subset.

J Additional Gradient-Geometry Analyses

J.1 Decile-Level Gradient Probe

The anchor/explorer split is a coarse partition. To test whether this spectrum is genuinely structured along the entropy axis rather than arising only from an extreme bottom–top contrast, we perform a decile-level gradient probe. We sort response tokens by attention entropy within each response, divide them into ten entropy deciles, compute the gradient induced by each decile under the same all-token-mean normalization, and compare each decile gradient to the full-token gradient using the projection-ratio diagnostic.

Figure 25 refines the coarse anchor–explorer view by showing how gradient contribution varies across the full entropy spectrum. Rather than collapsing tokens into only two groups, we measure the projection ratio of each entropy decile across training. This reveals a structured but non-monotonic pattern: upper-entropy deciles often contribute larger effective update components, especially in early-to-middle training, but low- and middle-entropy deciles remain non-negligible and become more prominent at other stages.

This decile-level view supports two conclusions. First, entropy is not merely a binary partitioning heuristic; it defines a continuous axis along which token groups exhibit systematically different optimization roles. Second, the spectrum is stage-dependent rather than strictly monotonic. If useful gradient contribution were concentrated in a fixed entropy region, one could safely train only that subset. Instead, the decile probe shows that effective update mass is distributed across the spectrum and shifts over training, motivating entropy-aware soft reweighting rather than fixed hard masking.

J.2 Online Directional-Stability Statistics

Section 4 analyzes gradient geometry using time-series diagnostics relative to the full-token update. Here we provide an additional online summary of directional stability. Specifically, we summarize the cosine-similarity trajectory between each subset gradient and the full-token gradient using its standard deviation and coefficient of variation (CV) across training.

For a diagnostic time series $\{c_s\}$, where c_s denotes the cosine similarity at probe step s , we define the online coefficient of variation as

$$CV(s) = \frac{\text{Std}(\{c_\tau : \tau \leq s\})}{|\text{Mean}(\{c_\tau : \tau \leq s\})| + \epsilon},$$

where ϵ is a small constant used only to avoid division by zero at the earliest steps. STD measures the absolute fluctuation of directional alignment, whereas CV measures fluctuation relative to the average alignment level. A large cosine CV therefore indicates that a subset gradient is directionally non-stationary relative to its typical agreement with the full-token update.

Figure 24 shows that random-20% subsets have the lowest cosine STD and CV throughout training. This is consistent with their role as noisy but stable sparse approximations of the full-token update. Entropy-defined subsets exhibit substantially larger directional non-stationarity. Anchor gradients show the largest cosine variation, which is consistent with the trajectory-level observation that they are strongly aligned early in training but progressively lose alignment as training proceeds. Thus, the large online variation of anchors reflects a systematic drift in their optimization role rather than purely stochastic instability.

Explorer gradients also show higher cosine variation than random subsets, although their STD/CV is lower than that of anchors in this statistic. This suggests that explorer-only instability should not be characterized simply as the largest short-term fluctuation in cosine similarity. Rather, together with the cosine trajectory in Figure 4, the result supports a more nuanced view: random subsets are directionally stable sparse estimators, anchors undergo strong temporal drift, and explorers provide directionally less reliable update components that pass through a low-alignment middle phase.

K Additional Details for the Dynamic Entropy-Aware Reweighting Intervention

This appendix gives the implementation details for the dynamic entropy-aware soft-reweighting intervention in Section 5. The main paper describes the intervention abstractly as a Low2High transition from low-entropy emphasis to high-entropy emphasis. Here we provide the exact instantiation used in our experiments. This schedule is used as a controlled validation probe for the diagnostic, not as a fully tuned algorithmic recipe. Static and reverse High2Low controls and remaining schedule sensitivity are discussed below and in the limitations.

Schedule instantiation. We use one fixed continuous weighting rule for the main dynamic-reweighting runs. The reweighter uses the decision attention entropy for each generated token: if the captured attention-entropy tensor includes the prompt-final position followed by response-token positions, the reweighting score for response token t uses the entropy at the generation step for that token.

For all valid response tokens \mathcal{V} in the current rollout batch, normalized decision attention entropy is converted into a temperature-scaled softmax score,

$$\alpha_t = \frac{\exp(H_t/\tau - c)}{\sum_{u \in \mathcal{V}} \exp(H_u/\tau - c) + \epsilon}, \quad c = \max_{u \in \mathcal{V}} H_u/\tau. \quad (26)$$

We then rescale this score over the same valid-token set,

$$\bar{\alpha}_t = \frac{\alpha_t - \min_{u \in \mathcal{V}} \alpha_u}{\max_{u \in \mathcal{V}} \alpha_u - \min_{u \in \mathcal{V}} \alpha_u + \epsilon}, \quad (27)$$

and assign the token weight by interpolation:

$$w_t^{(s)} = (1 - \bar{\alpha}_t)w_{\text{low}}(s) + \bar{\alpha}_t w_{\text{high}}(s). \quad (28)$$

The schedule is not selected separately for individual benchmarks. Let S_{warm} denote the warmup length and $r_s = \min(s/S_{\text{warm}}, 1)$ denote clipped warmup progress. We instantiate $w_{\text{low}}(s)$ and $w_{\text{high}}(s)$ as monotonic linear functions of r_s :

$$w_{\text{low}}(s) = w_{\text{low}}^{\text{start}} + r_s (w_{\text{low}}^{\text{end}} - w_{\text{low}}^{\text{start}}), \quad (29)$$

$$w_{\text{high}}(s) = w_{\text{high}}^{\text{start}} + r_s (w_{\text{high}}^{\text{end}} - w_{\text{high}}^{\text{start}}). \quad (30)$$

For the main Low2High intervention, we use $w_{\text{low}}^{\text{start}} = 1.0$, $w_{\text{low}}^{\text{end}} = 0.0$, $w_{\text{high}}^{\text{start}} = 0.0$, and $w_{\text{high}}^{\text{end}} = 1.0$. Thus low-entropy tokens receive larger weights early in training and high-entropy tokens receive larger weights after warmup. Intermediate tokens receive intermediate weights determined by their entropy-softmax scores. The computed weights multiply the token-level GRPO advantages; the actor loss uses all-token-weighted normalization, so the denominator remains the number of valid response tokens rather than the sum of weights.

Table 12: Per-seed benchmark results for full-token DAPO and Layer-20 entropy-aware reweighting on Qwen3-8B-Base. These runs underlie the mean \pm std values reported for the Layer-20 row in Table 1.

Method	Seed	AIME	OlympiadBench	Minerva	MATH	Avg.
Full-token DAPO	1	4.86	35.43	24.95	72.37	34.40
Full-token DAPO	2	6.01	33.35	27.32	72.73	34.85
Full-token DAPO	3	6.62	33.94	24.80	70.30	33.92
Entropy reweighting (Layer 20)	1	10.45	37.42	27.88	75.06	37.70
Entropy reweighting (Layer 20)	2	10.45	35.17	27.09	72.40	36.28
Entropy reweighting (Layer 20)	3	8.35	36.85	29.69	75.00	37.47

Table 13: Implementation details of the dynamic entropy-aware reweighting intervention. The same configuration is used across all benchmarks for a given run.

Item	Setting
Entropy score	Normalized attention entropy
Entropy source	Decision entropy for each generated token
Entropy layer	Layer 20 for controlled mid-layer runs; varied only in entropy-source comparisons
Softmax temperature	0.8
Weight signal	Batch-wise softmax over valid response-token entropy
Interpolation score	Min-max rescaled softmax score over valid tokens
Weight map	$(1 - \bar{\alpha}_t)w_{\text{low}} + \bar{\alpha}_t w_{\text{high}}$
Token coverage	All valid response tokens receive continuous weights
Main schedule	Low2High
Warmup length	80 steps
w_{low} init \rightarrow target	1.0 \rightarrow 0.0
w_{high} init \rightarrow target	0.0 \rightarrow 1.0
Applied quantity	Token-level GRPO advantages
Loss normalization	All-token-weighted normalization
Schedule selection	Fixed across benchmarks

K.1 Multi-Seed Robustness of Entropy-Aware Reweighting

To assess whether the gain from the entropy-aware reweighting intervention is driven by a favorable training seed, we repeat the primary controlled intervention comparison with multiple independent training seeds. This robustness check uses the fixed Layer-20 mid-layer entropy source, which is the same entropy source used for the schedule ablations. The shallow- and deep-layer rows in Table 1 are instead used to test entropy-source sensitivity. All runs use the same base model, training data, reward verifier, rollout configuration, optimization hyperparameters, and evaluation protocol as the main experiments; the only differences are the random seed and, for the reweighting variant, the token-weighting rule.

The Layer-20 row in the main table reports the corresponding mean \pm standard deviation. Table 12 provides the underlying per-seed benchmark results. This robustness check is intended to verify that the observed improvement of the controlled mid-layer reweighting setting is not an artifact of a single favorable run.

The multi-seed results provide a robustness check for the fixed Layer-20 intervention comparison. Since Layer-20 entropy-aware reweighting improves the mean held-out average over full-token DAPO across seeds, this supports the interpretation that the attention-entropy diagnostic captures actionable token-level structure rather than a single-run artifact. At the same time, we treat this result as evidence for the diagnostic and the optimization-spectrum analysis, rather than as an exhaustive claim that the particular hand-specified schedule or entropy-source layer is globally optimal.

Table 14: Soft-reweighting schedule ablation on Qwen3-8B-Base using the fixed Layer-20 entropy source. “Avg.” denotes the arithmetic mean over AIME, OlympiadBench, Minerva, and MATH. “Avg. w/o AIME” denotes the average over OlympiadBench, Minerva, and MATH only.

Variant	Early emphasis	Late emphasis	AIME	OlympiadBench	Minerva	MATH	Avg.	Avg. w/o AIME
Full-token DAPO	uniform	uniform	5.83	34.24	25.69	71.80	34.39	43.91
Static anchor-biased	low entropy	low entropy	5.78	34.18	25.80	71.23	34.25	43.74
Static explorer-biased	high entropy	high entropy	5.59	33.97	25.88	77.60	35.76	45.82
Dynamic Low2High (main)	low entropy	high entropy	9.75	36.48	28.22	74.15	37.15	46.28
Dynamic High2Low (ablation)	high entropy	low entropy	3.78	38.84	29.58	75.18	36.85	47.87

K.2 Reweighting Schedule Ablation

We further ablate the reweighting schedule used in the entropy-aware soft-reweighting intervention under the fixed Layer-20 entropy source. All variants use the same decision-attention entropy source, softmax temperature, continuous advantage reweighting rule, and all-token-weighted normalization as the controlled mid-layer intervention; they differ only in how the low- and high-entropy endpoint weights are assigned over training.

Table 14 compares static and dynamic weighting strategies on Qwen3-8B-Base. The static variants test whether the benefit can be explained by a fixed preference for one entropy regime. Static anchor-biased reweighting emphasizes low-entropy tokens throughout training and performs close to the full-token DAPO baseline, suggesting that a persistent low-entropy preference preserves stability but does not sufficiently expand coverage. Static explorer-biased reweighting improves the average mainly through MATH, but does not improve AIME, indicating that emphasizing high-entropy tokens alone is not a reliable strategy for harder reasoning benchmarks.

The dynamic variants test whether the temporal order of entropy-aware allocation matters. Among the Layer-20 schedules we tested, the **Low2High** schedule is the main controlled intervention and the most effective schedule within this fixed-layer ablation: it achieves the best average in this ablation, improving the held-out average from 34.39 to 37.15, with gains on all four benchmarks in the Layer-20 setting. This Layer-20 schedule result corresponds to the mid-layer row in Table 1; the shallow- and deep-layer rows vary the entropy source rather than the schedule. We interpret the schedule result as evidence that gradually reallocating weight along the attention-entropy spectrum can be more effective than using a fixed endpoint bias. In particular, starting from the lower-entropy side provides a more stable early optimization regime, while later increasing the emphasis on higher-entropy tokens allows the model to access broader but more volatile signals after the training trajectory has become less fragile.

The reverse **High2Low** schedule is an ablation. It also improves the average over the full-token baseline and obtains the highest average when AIME is excluded, showing that the gain is not simply tied to one fixed static bias. However, it substantially underperforms on AIME. This suggests that exposing training to high-entropy, directionally volatile signals too early can make the initial optimization trajectory less reliable, which may prevent the schedule from improving consistently across all benchmarks.

Overall, these ablations support a conservative conclusion: entropy-aware temporal reallocation is useful, and Low2High is the strongest schedule among the tested Layer-20 variants. However, this experiment is intended as an exploratory validation intervention rather than an exhaustive search over scheduling strategies. We did not further explore whether alternative transition shapes, transition timings, entropy thresholds, or weighting functions could yield stronger results. Therefore, the result should not be interpreted as evidence that Low2High is globally optimal; instead, it shows that attention-entropy-aware temporal reallocation can be beneficial under the tested fixed-layer schedules.

Training-curve comparison. Figure 26 provides a trajectory-level view of the dynamic schedule ablation in Table 14. On the held-out average, both dynamic schedules improve over the full-token DAPO baseline during training, suggesting that temporally reallocating token-level learning signal along the attention-entropy spectrum can be beneficial. The reverse High2Low schedule rises quickly and remains competitive on the aggregate average, which indicates that the benefit is not simply due to one static low-entropy or high-entropy bias.

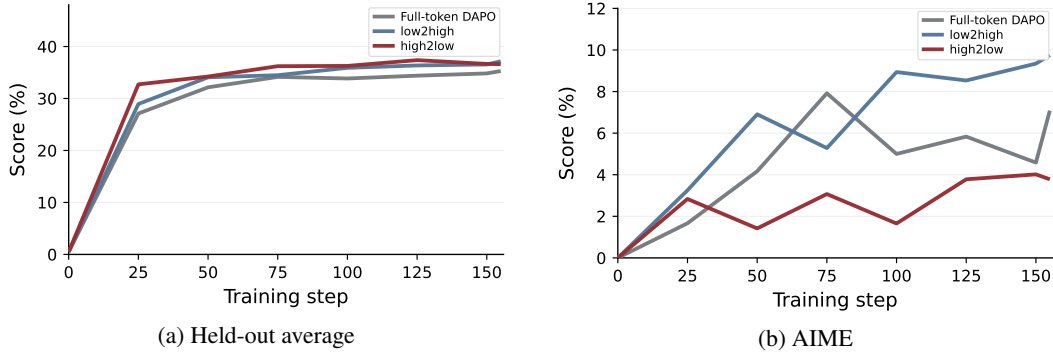


Figure 26: Training-curve comparison between the Low2High schedule and the reverse High2Low schedule under the fixed Layer-20 entropy source. The held-out average shows that both dynamic schedules can improve over full-token DAPO during training, indicating that entropy-aware temporal reallocation is more useful than a fixed uniform allocation. However, the AIME trajectory reveals a sharper distinction: Low2High achieves stronger late-stage AIME performance, whereas High2Low remains substantially weaker on this harder benchmark. This supports the interpretation that emphasizing high-entropy tokens too early may expose the model to more volatile signals before a stable optimization backbone has formed.

The AIME trajectory, however, reveals an important difference between the two temporal orders. Low2High consistently achieves stronger late-stage AIME performance, while High2Low remains much weaker on this harder benchmark. This pattern is consistent with the anchor-explorer interpretation: starting from low-entropy tokens provides a more stable early optimization regime, whereas shifting weight toward higher-entropy tokens later allows the model to access broader but more volatile reasoning signals after the trajectory has become less fragile. In contrast, emphasizing high-entropy tokens from the beginning can hurt the hardest-benchmark trajectory, even if it improves the aggregate average on easier or less brittle benchmarks.

We therefore interpret Figure 26 as trajectory-level support for the Layer-20 schedule-ablation conclusion rather than as an exhaustive schedule-selection result. Low2High is the strongest schedule among the tested Layer-20 variants, especially on AIME, but we do not claim that it is globally optimal over all possible transition shapes, timings, entropy temperatures, or weighting functions.

K.3 Entropy-Source Layer Sensitivity

The main analyses use Layer 20 as a fixed mid-layer attention-entropy probe. This choice is made to keep token grouping, support-concentration statistics, entropy dynamics, gradient-geometry diagnostics, and intervention comparisons under a single consistent mechanistic lens. It is not intended to claim that Layer 20 is the globally optimal entropy source.

To examine whether the intervention depends strongly on this fixed-layer choice, we compare representative shallow, middle, and final-layer entropy sources: Layer 8, Layer 20, and Layer 31. Layer indices follow our implementation convention, where Layer 31 corresponds to the final transformer layer. All other settings are kept unchanged, including the training data, reward verifier, rollout configuration, optimization hyperparameters, Low2High reweighting schedule, and strict exact-match evaluation protocol. The only difference is the layer from which normalized attention entropy is computed.

The corresponding results are reported in Table 1. The entropy-aware intervention remains effective under all three entropy-source layers, suggesting that the diagnostic is not tied to the specific Layer-20 probe used in the main mechanistic analyses. All three representative entropy sources improve over full-token DAPO on the held-out average and on every benchmark, but they expose different optimization profiles: Layer 8 achieves the strongest average and Minerva performance, Layer 20 gives the strongest AIME and MATH performance among the entropy-source rows, and Layer 31 gives the strongest OlympiadBench performance. This suggests that optimization-relevant attention-entropy structure can emerge across the depth of the model, while different depths may emphasize different parts of the reasoning signal.

Table 15: Supporting transfer checks for the entropy-aware reweighting intervention on additional models. Results use the same training data, reward, rollout, and evaluation protocol as the primary Qwen3-8B-Base comparison. These runs are intended as supporting evidence rather than a claim of universal effectiveness across model families.

Model	Full-token avg.	Soft avg.	AIME(Full-token)	AIME(Soft)
Qwen3-14B-Base	37.49	41.06	10.69	11.83
Qwen2.5-7B	30.82	34.47	5.27	7.61

We interpret this result conservatively. Since this is a representative three-layer check rather than a full layer-wise sweep, it should not be read as evidence that Layer 8 is universally optimal. Rather, it shows that entropy-source selection is an important design dimension and that useful attention-entropy signals can appear outside the fixed Layer-20 probe. A systematic study of layer selection, neighboring-layer stability, and multi-layer entropy aggregation is left for future work.

K.4 Intervention Transfer to Additional Models

The main paper reports Qwen3-8B-Base as the primary model to keep the comparison controlled. To examine whether the effect of entropy-aware soft reweighting is specific to this model, we further evaluate the same intervention on additional model families under the same data, reward, rollout, and evaluation protocol.

Table 15 provides supporting transfer checks on the tested models. On Qwen3-14B-Base, soft reweighting improves the held-out average from 37.49 to 41.06, with AIME increasing from 10.69 to 11.83. On Qwen2.5-7B, it improves the average from 30.82 to 34.47, with AIME increasing from 5.27 to 7.61. These results suggest that the benefit of entropy-aware soft reweighting is not limited to the primary Qwen3-8B-Base setting, but also appears on both a larger Qwen3 model and an earlier Qwen2.5 model.

We emphasize that these transfer results are intended as controlled supporting evidence rather than a claim of universal effectiveness across all model families. Nevertheless, the consistent gains across model scale and generation provide additional support for the anchor-explorer interpretation and for using attention entropy as a practical signal for token-level reweighting.

L Broader Impact.

This work studies token-level diagnostics and allocation strategies for RL-based reasoning post-training. Potential positive impacts include improving the interpretability, stability, and compute efficiency of reasoning-model training. Potential negative impacts follow from the broader improvement of reasoning capabilities in language models, which may make misuse such as automated problem solving, deceptive reasoning, or unsafe downstream deployment more effective if such models are released without appropriate safeguards. Our work does not release a new model, dataset, or user-facing system, and all experiments are conducted on mathematical-reasoning benchmarks. We recommend that any deployment of entropy-aware training methods be accompanied by standard model-safety evaluation, misuse monitoring, and domain-specific risk assessment.

M Existing Assets and Licenses

This work uses existing open models, datasets, benchmarks, and software frameworks obtained from Hugging Face Hub or the corresponding official repositories. We credit the original creators through citations in the main paper and appendix, and we use these assets only for research experiments under the licenses or terms specified by their Hugging Face model cards, dataset cards, or official repositories. We do not redistribute third-party model checkpoints, datasets, or code as new paper assets.

The main existing assets used in this work include the Qwen model family, VeRL, the DAPO recipe, DeepScaleR, MATH, AIME, OlympiadBench, and Minerva Math. In particular, the Qwen model checkpoints are used from the official Qwen Hugging Face repositories under the Apache-2.0

license. VeRL is used under the Apache-2.0 license. The DeepScaleR-Preview-Dataset Hugging Face release is listed under the MIT license. The MATH data are loaded from the Hugging Face HuggingFaceH4/MATH release, which is listed under the MIT license. The AIME evaluation data are loaded from the Hugging Face BytedTsinghua-SIA/AIME-2024 release, which is listed under the Apache-2.0 license. OlympiadBench is loaded from the Hugging Face Hothan/OlympiadBench release, which is listed under the Apache-2.0 license. Minerva Math is loaded from the Hugging Face svc-huggingface/minerva-math release, which is listed under the MIT license.

The DAPO recipe is used as an algorithmic and implementation reference for RLVR training, together with the VeRL-based training framework. We do not use or redistribute any third-party asset beyond the research-use scope specified by the corresponding Hugging Face cards or official repositories.

LLM Usage Disclosure

We used Claude as an auxiliary tool to assist with language editing, exploratory data analysis, and visualization scripting. The model was used to help improve grammar, spelling, and word choice; inspect experimental logs; draft plotting code; and generate figure layouts. All numerical results, statistical summaries, plots, and scientific interpretations reported in the paper were verified by the authors against the original experiment outputs. Claude was not used to generate training data, labels, model outputs for evaluation, or paper claims without author verification.